

RESEARCH PAPER



## Reducing INS-IGF1 signaling protects against non-cell autonomous vesicle rupture caused by SNCA spreading

Carl Alexander Sandhof<sup>1</sup>, Simon Oliver Hoppe<sup>1</sup>, Silke Druffel-Augustin<sup>1</sup>, Christian Gallrein<sup>2</sup>, Janine Kirstein<sup>2</sup>, Cindy Voisine<sup>3</sup>, and Carmen Nussbaum-Krammer<sup>1</sup>

<sup>1</sup>Center for Molecular Biology of Heidelberg University (ZMBH) and German Cancer Research Center (DKFZ), DKFZ-ZMBH Alliance, Heidelberg, Germany; <sup>2</sup>Department of Molecular Physiology and Cell Biology, Leibniz-Institute for Molecular Pharmacology (FMP) im Forschungsverbund Berlin e.V., Berlin, Germany; <sup>3</sup>Department of Biology, Northeastern Illinois University, Chicago, IL, USA

### ABSTRACT

Aging is associated with a gradual decline of cellular proteostasis, giving rise to devastating protein misfolding diseases, such as Alzheimer disease (AD) or Parkinson disease (PD). These diseases often exhibit a complex pathology involving non-cell autonomous proteotoxic effects, which are still poorly understood. Using *Caenorhabditis elegans* we investigated how local protein misfolding is affecting neighboring cells and tissues showing that misfolded PD-associated SNCA/ $\alpha$ -synuclein is accumulating in highly dynamic endo-lysosomal vesicles. Irrespective of whether being expressed in muscle cells or dopaminergic neurons, accumulated proteins were transmitted into the hypodermis with increasing age, indicating that epithelial cells might play a role in remote degradation when the local endo-lysosomal degradation capacity is overloaded. Cell biological and genetic approaches revealed that inter-tissue dissemination of SNCA was regulated by endo- and exocytosis (neuron/muscle to hypodermis) and basement membrane remodeling (muscle to hypodermis). Transferred SNCA conformers were, however, inefficiently cleared and induced endo-lysosomal membrane permeabilization. Remarkably, reducing INS (insulin)-IGF1 (insulin-like growth factor 1) signaling provided protection by maintaining endo-lysosomal integrity. This study suggests that the degradation of lysosomal substrates is coordinated across different tissues in metazoan organisms. Because the chronic dissemination of poorly degradable disease proteins into neighboring tissues exerts a non-cell autonomous toxicity, this implies that restoring endo-lysosomal function not only in cells with pathological inclusions, but also in apparently unaffected cell types might help to halt disease progression.

**Abbreviations:** AD: Alzheimer disease; BM: basement membrane; BWM: body wall muscle; CEP: cephalic sensilla; CLEM: correlative light and electron microscopy; CTNS-1: cystinosin (lysosomal protein) homolog; DA: dopaminergic; DAF-2: abnormal dauer formation; ECM: extracellular matrix; FLIM: fluorescence lifetime imaging microscopy; fps: frames per second; GFP: green fluorescent protein; HPF: high pressure freezing; IGF1: insulin-like growth factor 1; INS: insulin; KD: knockdown; LMP: lysosomal membrane permeabilization; MVB: multivesicular body; NOC: nocodazole; PD: Parkinson disease; RFP: red fluorescent protein; RNAi: RNA interference; sGFP: superfolder GFP; SNCA: synuclein alpha; TEM: transmission electron microscopy; TNTs: tunneling nanotubes; TCSPC: time correlated single photon counting; YFP: yellow fluorescent protein.

### ARTICLE HISTORY

Received 19 November 2018  
Revised 2 July 2019  
Accepted 11 July 2019

### KEYWORDS

Alpha-synuclein; aging; intercellular spreading; lysosomal homeostasis; lysosomal membrane permeabilization; neurodegenerative diseases; non-cell autonomous toxicity; proteostasis


### Introduction

Loss of protein homeostasis (proteostasis) and subsequent accumulation of protein aggregates is a hallmark of aging and linked to prevalent age-related diseases, such as Alzheimer disease (AD) or Parkinson disease (PD) [1–3]. Although most neurodegenerative diseases are characterized by a selective loss of specific highly vulnerable neurons, converging damage within neighboring cells strongly contributes to pathogenesis [4–7]. Studies in numerous disease models have revealed that a tissue-specific expression of aggregation-prone proteins is sufficient to cause a non-cell autonomous toxicity in surrounding cells [4,5,7,8]. Besides indirectly impacting nearby tissue by affecting the function of

expressing cells, mounting reports demonstrate that misfolded proteins themselves are secreted and spread to neighboring cells [9,10].

To counteract dysfunction and death of individual cells, a sophisticated protein quality control system that is well adapted to the cell type-specific proteome, maintains proteostasis [11]. This is particularly essential for post-mitotic cells, such as skeletal muscles or neurons, which have limited regenerative capacity. Since a cell type- or tissue-specific damage can have an impact upon the whole organism, metazoans also need to regulate the proteostasis network beyond the immediately affected cell to ensure survival of the species [11–14]. Recent studies revealed that proteostasis

**CONTACT** Carmen Nussbaum-Krammer  [c.nussbaum@zmbh.uni-heidelberg.de](mailto:c.nussbaum@zmbh.uni-heidelberg.de)  Center for Molecular Biology of Heidelberg University (ZMBH) and German Cancer Research Center (DKFZ), DKFZ-ZMBH Alliance, Im Neuenheimer Feld 282, D-69120 Heidelberg, Germany

 Supplementary material for this article can be accessed [here](#).

© 2019 The Author(s). Published by Informa UK Limited, trading as Taylor & Francis Group.  
This is an Open Access article distributed under the terms of the Creative Commons Attribution-NonCommercial-NoDerivatives License (<http://creativecommons.org/licenses/by-nc-nd/4.0/>), which permits non-commercial re-use, distribution, and reproduction in any medium, provided the original work is properly cited, and is not altered, transformed, or built upon in any way.

is indeed orchestrated at the organismal level. A sperm to oocyte signaling activates lysosomal function in oocytes to clear protein aggregates and avoid transmitting damage to the progeny [15]. Moreover, multiple stress responses that have been thought to function strictly cell autonomously, such as the heat shock response, are regulated in a non-cell autonomous manner [16–18]. A local activation of protective proteostasis components is sufficient to prevent protein aggregation in distant tissues and to delay organismal aging [19–23].

While there is increasing evidence for a non-cell autonomous regulation of stress response pathways, removal of protein aggregates and damaged organelles in adjacent cells or tissues has only recently been observed [24–26] and little is known about how this is regulated. Such non-cell autonomous processes may be implicated in the progression of neurodegenerative diseases and need further investigation.

In this study, we employed *C. elegans* to investigate the effects of local protein misfolding on neighboring cells and tissues and show that expression of PD-linked SNCA/ $\alpha$ -synuclein in muscle cells resulted in an age-dependent accumulation of misfolded protein species in endo-lysosomal vesicles. Accumulating SNCA was eventually transferred into remote hypodermal cells, which was facilitated by genes regulating vesicle trafficking and extracellular matrix composition. Transfer into the hypodermis was also observed upon cell type-specific SNCA expression in dopaminergic (DA) neurons, suggesting that the epithelium functions in transcellular removal of lysosomal substrates of proteolytically compromised surrounding cells. The chronic transfer of SNCA species caused endocytic vesicle rupture, indicating that spreading of pathology in neurodegenerative diseases could be a consequence of the failed systemic attempt to eliminate hardly digestible lysosomal substrates. Lysosomal membrane integrity was preserved in long-lived *daf-2* mutant animals defective in INS (insulin)-IGF1 (insulin-like growth factor 1) signaling, suggesting that improving endo-lysosomal function might be a promising therapeutic strategy to treat age-related diseases.

## Results

### **SNCA misfolds and accumulates in tubular structures with aging**

To study the systemic effects of local protein misfolding in post-mitotic cells we established transgenic *Caenorhabditis elegans* lines expressing SNCA/ $\alpha$ -synuclein, which has a central role in the pathogenesis of PD and other synucleinopathies. The nematode *C. elegans* is a widely used simple metazoan animal model to study the toxicity of proteins associated with human neurodegenerative diseases and transgenic *C. elegans* models expressing SNCA have been used to screen for modifiers of aggregation and toxicity [27–29]. In these lines, SNCA has either been untagged or tagged with yellow or green fluorescent protein (Y/GFP) [27–29]. The fluorescence intensity of these dyes significantly decreases at lower pH [30], which would diminish SNCA detection in acidic organelles such as endosomes or lysosomes. Since

mounting evidence suggests that misfolded SNCA is primarily targeted to lysosomes [31–33] and insufficient lysosomal clearance of aggregated SNCA is a key mechanism in the pathogenesis of synucleinopathies [34], we tagged SNCA with monomeric red fluorescent protein (RFP), which is insensitive to the endosomal milieu [30,35,36]. Expression of SNCA was restricted to body wall muscle (BWM) cells using the *myo-3* gene promoter for myosin heavy chain.

Besides exhibiting a weaker diffuse cytosolic fluorescence in BWM cells, SNCA::RFP formed intense fluorescent puncta, which have also been described in earlier studies (Figure 1A) [27,28]. Remarkably, in addition to previous reporter patterns in transgenic *C. elegans* lines, SNCA::RFP was also detected in spherical and tubular structures (Figure 1A) that were highly mobile and dynamic undergoing frequent fusion and fission events (Video S1), suggesting that they might represent endosomal vesicles. These SNCA::RFP shapes were not detected in embryos and L1 larvae, and initially observed in L2 larvae (Figure 1B), where spherical patterns were more abundant in early larval development. In later development and during aging of adult animals, SNCA::RFP was found in tubular structures that increased in size and number (Figure 1B,C).

To obtain information about the aggregation state of SNCA::RFP in adult animals, we took advantage of fluorescence lifetime imaging microscopy (FLIM) [37]. The specific fluorescence lifetime of fluorophores negatively correlates with the extent of aggregation, which allows tracking of aggregation dynamics of fusion proteins *in situ* [37,38]. Accordingly, we observed a significant decline of fluorescence lifetime of SNCA::RFP upon aging, indicating increased aggregation of SNCA::RFP (Figure 1C,D). This shift towards lower values, was especially pronounced between 4- and 5-d-old animals and correlated with increased occurrence of tubular structures (Figure 1C,D). Indeed, SNCA::RFP tubules exhibited a reduced fluorescence lifetime compared to the fluorescent cytoplasm in the background (Figure 1C). To further analyze the biochemical properties of SNCA::RFP aggregates in 5-d-old animals, we tested their solubility in different detergents [39]. The protein was extracted successively from whole worm lysates with different buffers containing first Tris-HCl only, then Tris-HCl with 1% Triton X-100, 1% sarkosyl, or 2% SDS, respectively (Figure 1E). The majority of SNCA::RFP was detected in the Tris-HCl and Triton X-100 soluble fractions, containing mostly soluble and membrane-bound proteins, while a smaller fraction was found in the sarkosyl soluble and SDS soluble fractions, indicating oligomeric or aggregated SNCA::RFP. In sum, this biochemical assay confirms the *in vivo* FLIM data that a significant portion of the protein is aggregating when expressed in *C. elegans*.

Fusing proteins to bulky fluorophores often raises the concern that this might affect the folding and subcellular localization of tagged proteins. To rule out potential artifacts, we assessed the aggregation state and subcellular distribution of RFP itself in more detail. In control animals expressing monomeric RFP fluorophore, the protein was only detected in the HCl soluble fraction after sequential extraction (Figure S1B) and the mean fluorescence lifetime was significantly higher, which was reflected by a diffuse cytosolic staining,

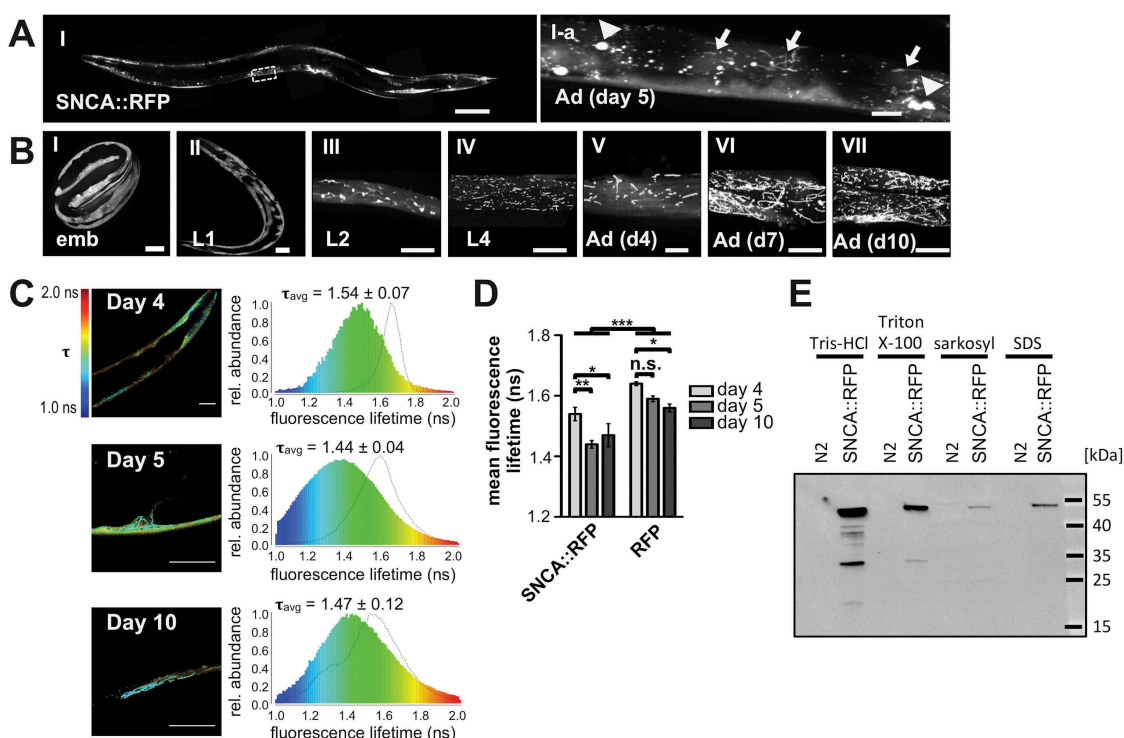


**Figure 1.** SNCA misfolds and accumulates in tubular structures with aging. (A,B) Collapsed confocal z-stacks of nematodes expressing SNCA::RFP in BWM cells. (A) SNCA::RFP is accumulating in spherical foci (arrowheads) and tubular structures (arrows) in 5-d-old animals. (I) Z projections along the length of the animal were stitched to create a high-resolution montage of an entire worm; scale bar: 100  $\mu$ m. (I-a) Zoom of boxed region in (I); scale bar: 10  $\mu$ m. (B) Images of nematodes expressing SNCA::RFP acquired at indicated developmental stages. The diffuse staining of SNCA in embryos and L1 larvae indicates soluble cytosolic protein. Accumulation of SNCA-positive tubular patterns first occurs between the L1 and L2 larval state and increases during development. Scale bars: 10  $\mu$ m. Emb: embryo; L1-L4: larval stage 1 to 4; Ad: adult. (C) Left images depict representative TCSPC-images of SNCA::RFP nematodes on day 4, 5 and 10 of life. Intensity-weighted fluorescence lifetime ( $\tau$ ) is indicated in false colors (decreasing from red to blue). Magnification of day 4 images was 630x, magnification of day 5 and 10 images were 2.000x. Scale bars: 20  $\mu$ m. Right panels represent the corresponding histograms showing the relative abundance of pixels exhibiting a certain fluorescence lifetime ( $\tau$ ), averaged over all acquired images ( $n = 10$ –20 for each time point). Dashed, black lines are fluorescence lifetime distributions of age-matched control nematodes expressing fluorophore (RFP) only. (D) Bar plots of mean fluorescence lifetime of SNCA::RFP and RFP at different ages. Data are shown as mean  $\pm$  SEM. Statistical analysis was done using two-way ANOVA with Bonferroni posttests. \* =  $p < 0.05$ , \*\* =  $p < 0.01$ , \*\*\* =  $p < 0.001$ . (E) Sequential extraction of SNCA::RFP with Tris-HCl buffer, and Tris-HCl buffer containing 1% Triton X-100, 1% sarkosyl and 2% SDS from lysates of 5-d-old animals reveals a small fraction of detergent insoluble SNCA::RFP.

indicating mostly soluble protein (Figure 1C,D, S1A and S1C). Albeit to a lesser extent than SNCA::RFP, the mean fluorescence lifetime of RFP decreased during aging, which correlated with a minor fraction of RFP accumulating in small spherical foci that likely consist of aggregated RFP (Figure S1A and S1C). However, the shape and number of RFP foci differed greatly at all ages and did not reveal either the prominent tubular structures or the level of aggregation as observed with SNCA::RFP (Figure 1, S1A and S1C). Moreover, SNCA tagged with Dendra2, another monomeric tag that can be visualized in endo-lysosomal vesicles [40], exhibits a similar morphology as SNCA::RFP (Figure S1D). Hence, the characteristic subcellular pattern observed with SNCA::RFP seems to be an intrinsic property of SNCA rather than a consequence of the RFP tag.

### SNCA accumulates in tubular endo-lysosomal vesicles

To characterize the properties of SNCA-positive structures, and to determine whether they correspond to vesicles, we investigated their ultrastructural morphology by correlative light and electron microscopy (CLEM) and in samples prepared for ultrastructural examination in transmission

EM (TEM) (Figure 2A). We made use of the CLEM preservation technique developed by Kukulski et al. [41]. This method utilizes cryo preservation techniques of high pressure freezing (HPF) and freeze substitution in a solution consisting of low amount of uranylacetate in acetone, which prevents the loss of fluorochrome fluorescence. Compared to conventional electron microscopy preservation, the samples have lower contrast, but the possibility to retain the fluorescent signal of FPs. To increase the contrast, we did freeze substitute some of the samples in a cocktail containing osmium tetroxide as well as uranyl acetate in order to get samples with higher membrane contrast and staining.

In our CLEM samples the rather weak fluorescent signal of diffuse cytosolic SNCA::RFP in 5-d-old animals was mainly lost after the HPF and freeze substitution procedure. However, the relative bright fluorescence of SNCA::RFP foci and tubules could be preserved and correlation showed that SNCA is present in tubular structures which appear as electron dense spherical and tubular vesicular structures (Figure 2A I-III). In the osmium treated samples, we readily identified the corresponding electron dense spherical and tubular structures (Figure 2A IV-VI). Moreover, in these samples, a membrane border was clearly



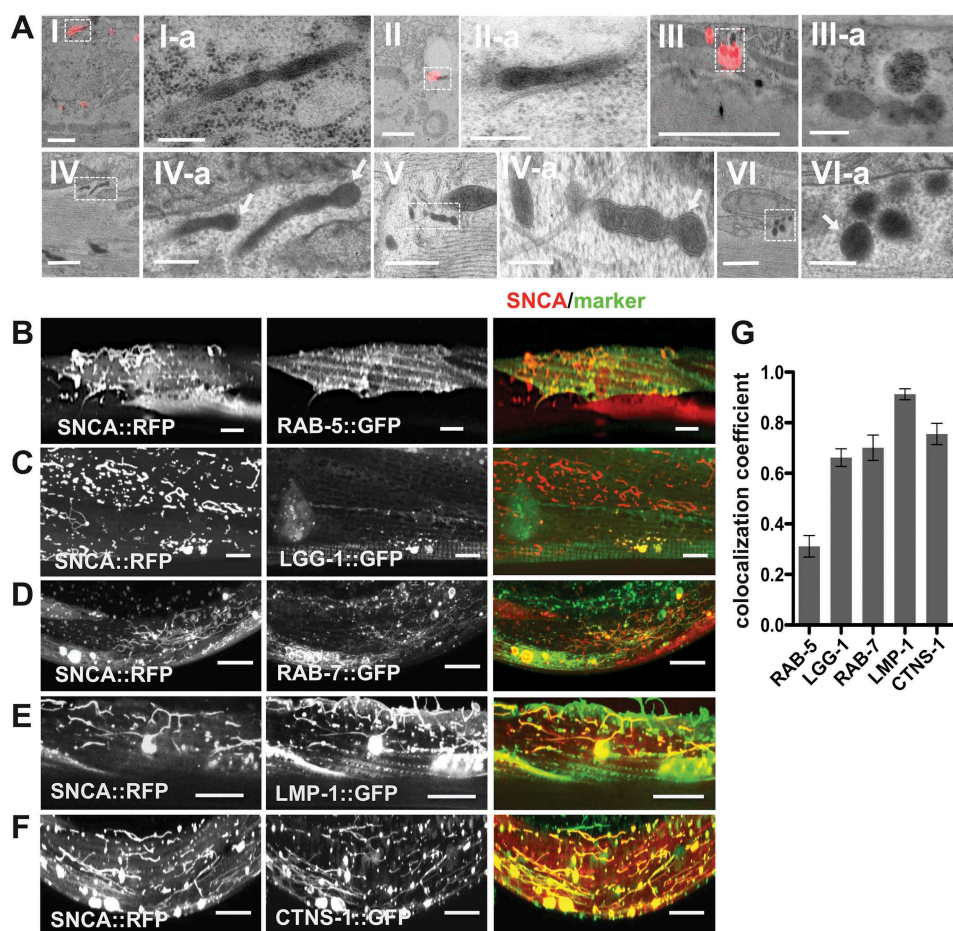


**Figure 2.** SNCA accumulates in tubular endo-lysosomal vesicles. (A) Images with light microscopy signal correlated on the electron micrographs (I-III) and osmium stained samples in TEM (IV-VI) from nematodes expressing SNCA::RFP in BWM cells. Scale bars: 1  $\mu$ m. (A). Zoom in of boxed region in corresponding picture. Scale bars: 200 nm. (I-III) After HPF samples were stained very gently during freeze substitution in order to preserve RFP fluorescence for CLEM. Grids with 90 nm thick sections were first imaged by fluorescent light microscopy. After staining with 3% uranyl acetate and Reynold's lead citrate, the identical areas were then imaged by TEM. SNCA::RFP colocalizes with spherical and tubular electron dense vesicles. (IV-VI) HPF samples of SNCA::RFP transgenic nematodes were subjected to osmium staining during freeze substitution, revealing that the electron dense spherical and tubular SNCA::RFP-positive structures are enclosed by a single membrane. (b-f) Collapsed confocal z-stacks of nematodes expressing the indicated proteins. 5-d-old animals were analyzed. Scale bars: 10  $\mu$ m. (B) SNCA::RFP colocalizes to a minor extent with RAB-5-positive early endosomes and (C) with LGG-1 (homolog of LC3)-positive autophagosomes. (D) SNCA::RFP partially localizes to RAB-7-positive late endosomes. (E,F) SNCA::RFP extensively colocalizes with LMP-1, a late endosomal/lysosomal membrane protein, and CTNS-1, a late endosomal/lysosomal amino acid transporter, respectively. (G) Quantification of SNCA::RFP colocalization with indicated vesicle markers using ZEN software. Data are shown as mean  $\pm$  SEM.

visible showing a typical double-contoured layer (Figure 2A IV-VI). The membranes at the vesicle ends often seem tangentially sectioned, indicating that the image depicts a section through a tubular structure, which extends beyond the section thickness of 70–90 nm.

Next, to determine the type of vesicles containing SNCA, we co-expressed various markers for cytosolic vesicles (Figure 2B–F). Colocalization was quantified by Zeiss Zen software (Figure 2G). A minor fraction of SNCA colocalized with RAB-5-positive early endosomes (Figure 2B). In contrast, spherical SNCA foci partially colocalized with LGG-1 (LC3, GABARAP and GATE-16 family), the *C. elegans* homolog of the autophagosome marker Atg8/LC3 (Figure 2C) and some spherical and tubular SNCA structures colocalized with RAB-7, a marker for multivesicular bodies (MVBs) and late endosomes (Figure 2D). Tubular SNCA structures colocalized extensively with LMP-1, a late endosomal and lysosomal membrane protein (Figure 2E), and with CTNS-1, a late endosomal/lysosomal cystine transporter [42] (Figure 2F).

These results indicate that SNCA accumulates in autophagy-related vesicles with lysosome-like properties, and by using an RFP tag to visualize SNCA, we were able to monitor a previously unrecognized endosomal fraction of SNCA in *C. elegans*.

### SNCA vesicle tubulation and movement depends on active trafficking along microtubules

Secretory vesicles have been shown to be transported to the plasma membrane along microtubules [43,44]. Therefore, we tested whether the movement of SNCA::RFP containing vesicles in BWM cells is mediated by microtubule-dependent trafficking by co-expressing EMTB::GFP, a GFP fusion protein containing the microtubule binding domain of MAP7/ensconsin as a tool for *in vivo* visualization of microtubule dynamics [45]. Indeed, SNCA::RFP vesicles colocalize with (Figure 3A) and move along microtubules (Video S2). To examine the dynamic properties of the SNCA::RFP containing vesicles, the ATP- and microtubule-

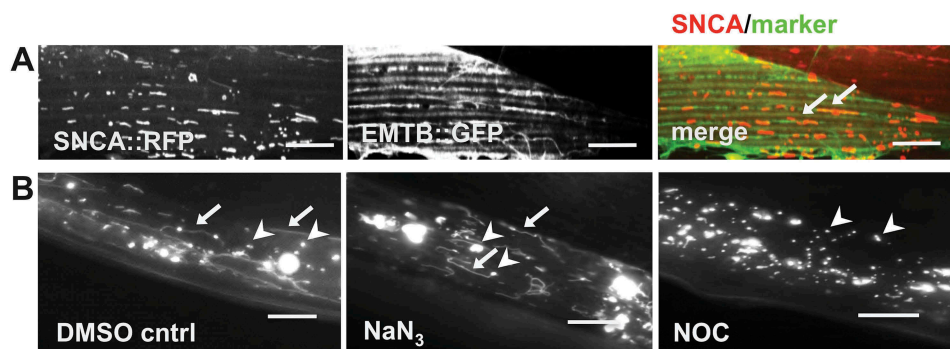


**Figure 3.** SNCA vesicle tubulation and movement depends on active trafficking along microtubules. (A) Collapsed confocal z-stacks of 5-d-old nematodes expressing SNCA::RFP together with EMTB::GFP, showing that vesicular SNCA colocalizes with microtubules (arrows). Scale bars: 10  $\mu\text{m}$ . (B) Collapsed z-stacks of wide field microscopy images of 5-d-old animals expressing SNCA::RFP after acute treatment with the indicated drugs. Note that tubular (arrows) and spherical (arrowheads) vesicles are visible after application of either DMSO solvent control or sodium azide ( $\text{NaN}_3$ ), whereas in nocodazole (NOC) treated animals only spherical vesicles are visible. Scale bars: 10  $\mu\text{m}$ .

dependent vesicular transport was inhibited by incubation with the metabolic inhibitor sodium azide ( $\text{NaN}_3$ ), which results in rapid depletion of intracellular ATP levels, and with nocodazole (NOC), a microtubule-depolymerizing agent. Upon acute drug treatments with either  $\text{NaN}_3$  or NOC, the dynamics of vesicular SNCA::RFP movement were inhibited, suggesting that the transport was ATP and microtubule-dependent, respectively (Videos S3-S5). In addition, only NOC treatment, but not ATP depletion, depolymerized microtubules (Figure S2), and caused SNCA::RFP vesicles to collapse from tubular into spherical shapes (Figure 3B, Video S5). Hence, SNCA vesicle tubulation and movement depends on active trafficking along microtubules within BWM cells. These results are consistent with observations that microtubules have distinct roles to determine the morphology of vesicles and to mediate their transport [44].

### SNCA spreads across a basement membrane and accumulates in epithelial tissue

Vesicular packaging and impaired lysosomal degradation has been suggested to have a critical role in donor cells for the secretion of SNCA [31,34,46–49]. To determine whether SNCA::RFP might be secreted and spread to neighboring tissues, we monitored the appearance of SNCA::RFP outside of BWM cells. We were able to detect the accumulation of SNCA::RFP mainly in the hypodermis (Figure 4B and Video S6), which was confirmed by co-expression of GFP under the control of a hypodermis-specific promoter (Figure 4C). The *C. elegans* hypodermis consists of a single epithelial layer that surrounds the animal and is separated from internal tissues such as BWM cells by the basement membrane (BM), an extracellular matrix (ECM) comprised of a single layer of collagen, laminin, fibronectin, and other long chain macromolecules [50]. Moreover, SNCA accumulated in endolysosomal vesicles of receiving hypodermal cells, as shown by colocalization with the lysosomal marker CTNS-1 that was also expressed in the hypodermis (Figure 4D).

We again aimed to examine the aggregation state of SNCA::RFP and the ultrastructural morphology of hypodermal SNCA::RFP vesicles by TEM. Since SNCA::RFP is not expressed in hypodermal cells, we were not able to detect the very weak fluorescent signal from the transmitted fraction of SNCA in FLIM or CLEM. However, by using conventional TEM, electron dense spherical and tubular structures were detected (Figure 4E), which resemble the SNCA::RFP containing vesicles described earlier in BWM (Figure 2A). Intriguingly, some of these vesicles exhibited not only a single, but also a double-membrane border, appearing as 5-contoured layer (low-high-low-high-low electron dense area) (Figure 4E II-a), indicating that they might result from autophagic processes or endocytosis of extracellular vesicles. Again, discontinuous membrane borders are indicative of tubular structures extending beyond the section thickness.

Monitoring and quantification of SNCA::RFP dissemination during development and aging revealed a dramatic transition between 4- and 5-d-old animals (corresponding to day 1 and day 2 of adulthood), where transmission of SNCA::RFP into the hypodermis went from rarely being detectable to an average of 80% of animals (Figure 4F,G). This implies that age-related processes might influence the inter-tissue transfer of SNCA. The abrupt onset of spreading was only marginally affected by SNCA::RFP expression levels (Figure 4H and S3). In contrast, the SNCA<sup>A53T</sup> variant, a point mutation linked to early onset PD and known to be more aggregation prone [51], was transmitted earlier with hypodermal SNCA::RFP being detected in 30% of animals on day 4 (Figure 4I). This correlated with increased aggregation and toxicity of the protein, as examined by detergent extraction assay (Figure 4K) and thrashing assay (Figure 4L), respectively. Hence, aggregation and toxicity appear to affect SNCA spreading.

Of note, neither the RFP tag alone, nor 40 polyglutamine repeats fused to RFP (polyQ40::RFP) accumulate in tubular lysosome-like vesicles or are detected in the hypodermis in 5-d-old animals at comparative levels (~10% vs. ~80%) (Figure S4), indicating that these effects are specifically asso-

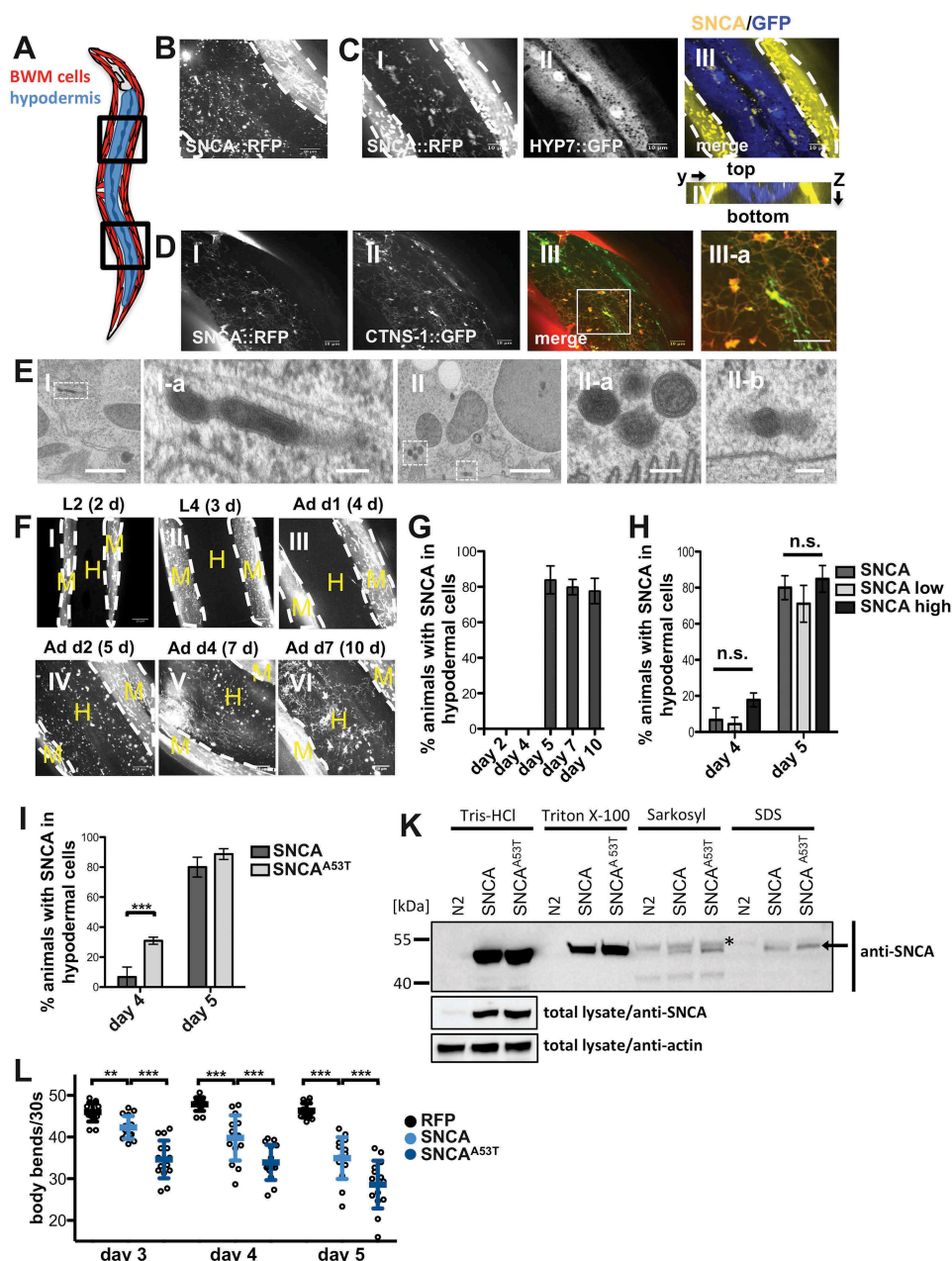


**Figure 4.** SNCA is able to cross a basement membrane and accumulates in epithelial tissue. (A) Schematic depiction of region of imaging in (B–D,F). (B–D,F) Collapsed confocal z-stacks of nematodes expressing indicated proteins. White dashed lines outline the borders of BWM cells. Scale bars: 10  $\mu$ m. (B) SNCA::RFP can be detected outside the borders of BWM cells. (C) GFP expressed in the hypodermis reveals the localization of SNCA inside hypodermal cells. (III–a) y-z orthogonal view of (III). (D) The lysosome marker CTNS-1 expressed in the hypodermis colocalizes with SNCA indicating that SNCA is accumulating in lysosomal vesicles after transmission. (E) TEM analysis of 5-d-old nematodes expressing SNCA::RFP in BWM cells, revealing electron dense spherical and tubular vesicles in hypodermal tissues, which are enclosed by a single or double membrane. Scale bars: 1  $\mu$ m (I+ II); 200 nm (Ia–IIb). (F) Inter-tissue transmission of SNCA is age-dependent. Images of nematodes expressing SNCA::RFP acquired at indicated time points during development and aging. Hypodermal SNCA can be detected in nematodes that are at least 5 d old. L2 and L4: larval stage 2 and 4; d: day; Ad: adult; M: muscle; H: hypodermis. (G–I) Quantification of animals with hypodermal SNCA harboring the indicated transgenes at indicated ages. (K) Sequential extraction of WT and A53T mutant SNCA::RFP with Tris-HCl buffer, and Tris-HCl buffer containing 1% Triton X-100, 1% sarkosyl and 2% SDS from lysates of 5-d-old animals detects both variants in detergent insoluble fractions. The SNCA<sup>A53T</sup> variant forms slightly more detergent insoluble material than the WT SNCA protein. The asterisk (\*) indicates an unspecific band, which migrates just above the SNCA-specific band in the sarkosyl fraction. In parallel, total lysates were probed with anti-SNCA and anti-actin antibodies to demonstrate equal protein concentrations. (L) Scatter dot plot showing the number of body bends (thrashes) of animals expressing the indicated transgenes during a 30 s swimming period in M9 at indicated ages. Expression of the SNCA<sup>A53T</sup> variant caused an accelerated decline of muscle function during aging. Data information: Data are shown as mean  $\pm$  SD. In (G, H and I) statistical analyses were done using two-way ANOVA with Bonferroni posttests. In (L) statistical analyses were done using two-way ANOVA with Holm-Sidak's multiple comparisons test. n. s. = not significant, \*\* =  $p < 0.01$ , \*\*\* =  $p < 0.001$ .

ciated with SNCA. These results suggest that the endolysosomal system is particularly vulnerable to the accumulation of misfolded SNCA, which is transferred from muscle cells into epithelial cells in an age-dependent manner.

### Reduced *INS-IGF1* signaling delays SNCA spreading

The striking age-dependence observed for SNCA spreading was further addressed in long-lived animals. In *daf-2(e1370)* *INS-*



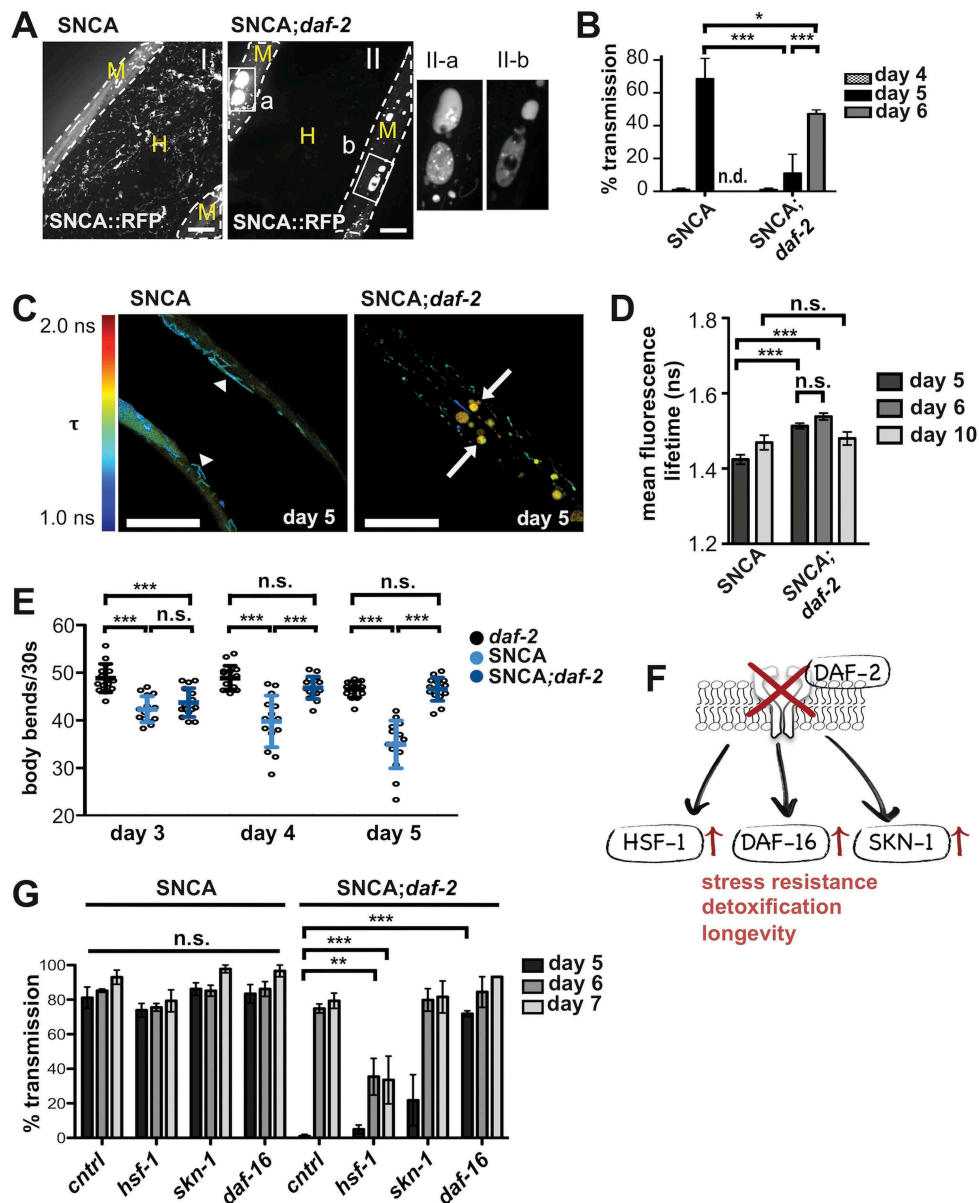


**Figure 5.** Reduced INS-IGF1 signaling delays SNCA spreading. (A) Collapsed z-stacks of the hypodermis of 5-d-old nematodes expressing SNCA::RFP in the WT or *daf-2(e1370)* mutant background. (II) Note the appearance of large MVB-like vesicles in SNCA;*daf-2* animals. (II-a and II-b) Zoom of boxed regions in (II). Scale bars: 10  $\mu$ m. (B) Quantification of SNCA transmission (number of animals that exhibit SNCA vesicles within the hypodermis) at indicated ages. n.d.: not determined. Reduced INS-IGF1 signaling in *daf-2* mutant animals suppresses the transmission of SNCA::RFP into the hypodermis on day 5. (C) Representative TCSPC-images of SNCA and SNCA;*daf-2* nematodes on indicated days of life. Intensity-weighted fluorescence lifetime ( $\tau$ ) is indicated in false colors (decreasing from red to blue). Note the presence of spherical SNCA containing vesicles (arrow) in *daf-2* mutant animals and the relatively high fluorescence lifetime of SNCA::RFP in these vesicles compared to the fluorescence lifetime of SNCA::RFP in tubular vesicles (arrowhead) of WT animals on day 5. Scale bars: 25  $\mu$ m. (D) Bar plots of mean fluorescence lifetime of SNCA::RFP in the WT and *daf-2* mutant background at different ages. (E) Scatter dot plot showing the number of body bends (thrashes) of animals harboring the *daf-2* mutation and/or expressing SNCA::RFP during a 30-s swimming period in M9 at indicated ages. Reduced insulin receptor function rescued the SNCA::RFP associated decline of muscle function. (F) Schematic depiction of stress response pathways downstream of DAF-2 receptor signaling. Reduced INS-IGF1 signaling increases the activity of the transcription factors HSF-1, DAF-16 and SKN-1, which regulate the expression of downstream genes that improve stress resistance, detoxification and prolong lifespan. (G) Quantification of SNCA::RFP transmission at indicated ages in WT and *daf-2* mutant animals upon RNAi-mediated KD of the indicated genes. KD of *daf-16* abolishes the *daf-2*-mediated suppression of SNCA::RFP spreading on day 5. Data information: In (B,E) data are shown as mean  $\pm$  SD. In (D,G) data are shown as mean  $\pm$  SEM. In (B,D,G) statistical analyses were done using two-way ANOVA with Bonferroni posttests. In (e) statistical analyses were done using two-way ANOVA with Holm-Sidak's multiple comparisons test. n. s. = not significant, \* =  $p < 0.05$ , \*\* =  $p < 0.01$ , \*\*\* =  $p < 0.001$ .

IGF1 receptor mutants, we observed an accumulation of large SNCA::RFP containing vesicles resembling MVBs and fewer tubular vesicles in donor BWM cells in comparison to the WT background (Figure 5A). This correlated with the suppression of the appearance of SNCA::RFP vesicles in the hypodermis in 5-d-old animals (Figure 5A,B). The delay in spreading correlated with a diminished aggregation (Figure 5C,D and S5) and toxicity

(Figure 5E) of SNCA::RFP in the *daf-2* mutant background. FLIM further revealed that the spherical vesicles in *daf-2* mutants contained less aggregated material than the vesicles with tubular shape in WT animals (Figure 5C). However, the suppression of spreading was only transient, and SNCA::RFP accumulated in the hypodermis up to WT levels the following day (Figure 5B,G), although aggregation was still

reduced and remained comparable in 5- and 6-d-old *daf-2* animals.

We next tested which of the pathway downstream of DAF-2 signaling might mediate the delay in SNCA spreading. Reduced INS-IGF1 signaling in *daf-2* mutants increases stress resistance and extends lifespan by upregulating the stress response transcription factors, HSF-1, DAF-16 and SKN-1 (Figure 5F). We quantified hypodermal SNCA::RFP in WT and *daf-2* mutant animals after silencing the respective genes by RNA interference (RNAi). While there were no effects on the amount of hypodermal SNCA::RFP in WT animals, the knockdown (KD) of *daf-16* completely reversed the *daf-2* dependent suppression of SNCA spreading in 5-d-old animals (Figure 5G). In contrast, *hsf-1* KD had an additive effect and further delayed and reduced SNCA::RFP dissemination in 6- and 7-d-old animals. Overall, these experiments revealed that decreased insulin receptor function delayed but did not abolish hypodermal accumulation of SNCA in a *daf-16* dependent manner.

### Reduced INS-IGF1 signaling suppresses SNCA-mediated endosomal rupture in receiving cells

To characterize the consequence of SNCA::RFP accumulation in endo-lysosomal vesicles, we used human LGALS3/galectin-3, a lectin that redistributes to damaged endo-lysosomal vesicles and forms puncta upon vesicle rupture [52–54]. In control animals, LGALS3 fused to superfolder GFP (sfGFP::LGALS3) was diffuse in the cytosol and puncta structures were rarely detected (Figure 6A,B). In contrast, co-expression of SNCA::RFP and the reporter in BWM cells resulted in a significant amount of LGALS3 foci formation in 4- and 5-d-old animals indicating vesicle damage (Figure 6A,B), confirming previous reports that misfolded SNCA ruptures endosomes [52,54]. We next examined a strain that expresses sfGFP::LGALS3 in the hypodermis to investigate the effect of SNCA::RFP spreading to receiving cells. In 4-d-old animals, sfGFP::LGALS3 puncta are detected infrequently in both control and SNCA expressing animals. However, in

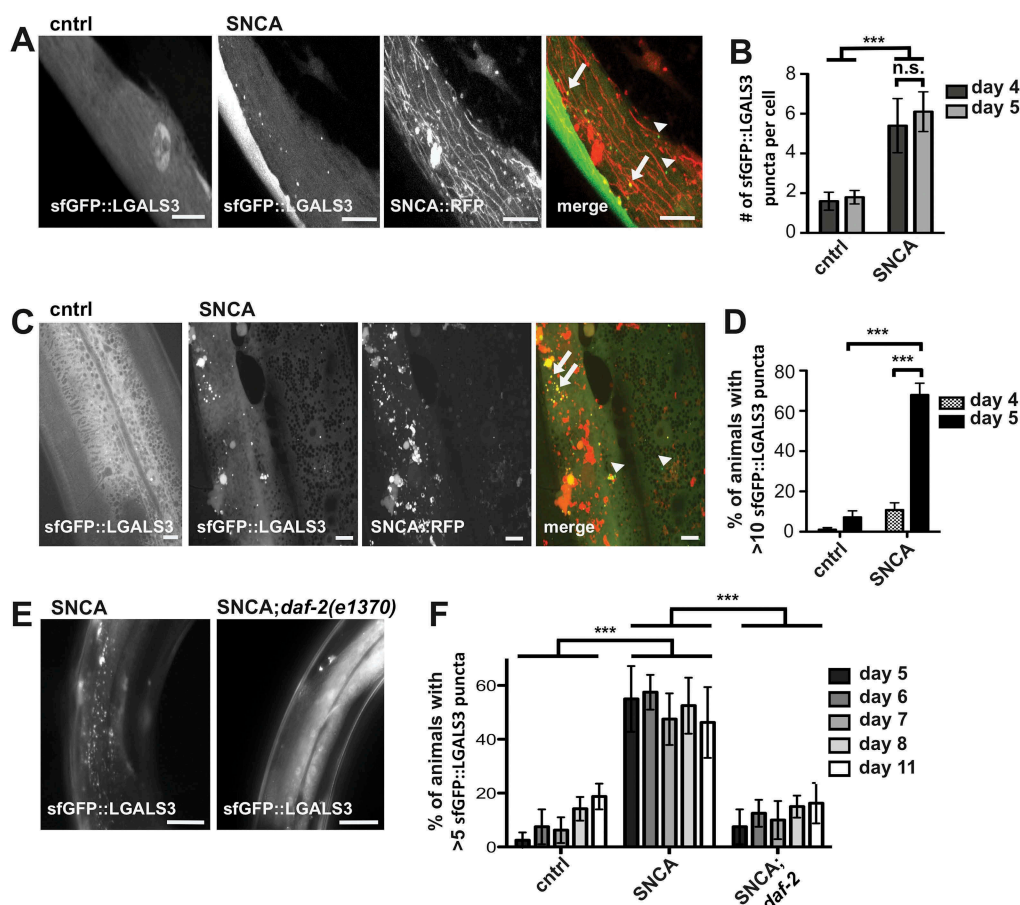


**Figure 6.** Reduced INS-IGF1 signaling suppresses SNCA-mediated endosomal rupture in receiving cells. (A,C) Collapsed confocal z-stacks of 5-d-old nematodes expressing indicated proteins or harboring indicated mutations. Arrows indicate colocalizing puncta, arrowheads mark non-colocalizing puncta in the merged images. Scale bars: 10  $\mu$ m. (A) Co-expression of SNCA::RFP and sfGFP::LGALS3 in BWM cells results in increased LGALS3 puncta formation. (B) Quantification of the number of sfGFP::LGALS3 puncta per cell shows that SNCA::RFP induces a comparable level of endo-lysosomal rupture in muscle cells of 4-d-old and 5-d-old animals. (C) In 5-d-old animals, sfGFP::LGALS3 puncta reveal endo-lysosomal leakage in hypodermal cells when SNCA::RFP is expressed in BWM cells, but not in control animals. (D) Quantification of animals with hypodermal sfGFP::LGALS3 foci reveals a striking increase in endo-lysosomal rupture in 5-d-old animals. (E) Collapsed z-stacks of 5-d-old nematodes expressing indicated proteins or harboring indicated mutations. Reduced INS-IGF1 signaling in *daf-2* mutant animals protects against lysosomal rupture. Scale bars: 100  $\mu$ m. (F) Quantification of animals with sfGFP::LGALS3 foci at indicated ages. Data information: In (B,D,F) data are shown as mean  $\pm$  SD. Statistical analyses were done using two-way ANOVA with Bonferroni posttests. n. s. = not significant, \*\* =  $p < 0.01$ , \*\*\* =  $p < 0.001$ .



5-d-old animals, high levels of sfGFP::LGALS3 puncta were detected in SNCA expressing animals, whereas the reporter remained diffuse in control animals (Figure 6C,D). This correlates with the onset of transmission of SNCA into the hypodermis in 5-d-old animals, and suggests that the SNCA::RFP-positive endo-lysosomal vesicles in hypodermal cells ruptured. We took advantage of this reporter and used sfGFP::LGALS3 puncta formation as indirect evidence for SNCA spreading. The co-expression of untagged SNCA in BWM cells was sufficient to cause a significant increase in sfGFP::LGALS3 puncta formation in the hypodermis of 5-d-old animals compared to control animals only expressing sfGFP::LGALS3 (Figure S6). This further confirmed that the observed phenotype can be attributed to SNCA and is not mediated by the RFP tag. In sum, the dissemination and accumulation of SNCA in the receiving epithelial tissue exerts non-cell autonomous toxicity.

In *daf-2* mutant animals, endosomal integrity was maintained not only in 5-d-old animals, when SNCA transmission is suppressed, but also in 6- and up to 11-d-old animals, when SNCA is found in the hypodermis to the same extent as in WT animals (Figure 5B,G). The fact that SNCA aggregation was comparable in 10-d-old WT and *daf-2* mutants (Figure 5D and S5) indicates that reduced INS-IGF1 signaling has dual effects: it delays protein transmission and suppresses leakage of aggregated SNCA from endocytic vesicles in receiving cells despite continued dissemination, suggesting an improvement in lysosomal protein turnover in donor and receiving tissues.

### SNCA spreading to the hypodermis does not involve transfer of intact endo-lysosomal vesicles through Tunneling Nanotubes (TNTs)

We next determined how SNCA is transmitted from BWM cells to the hypodermis, and considered several possibilities. Passive transfer would involve the non-selective release of SNCA from donor cells by cell death or through membrane pores, whereas active transport mechanisms would include ATP-dependent pathways such as vesicular transport through tunneling nanotubes (TNTs) or endo- and exocytosis. To test whether the release of SNCA::RFP occurs passively by the uncontrolled release of cytosolic contents due to membrane leakage and cell death, we co-expressed YFP together with SNCA::RFP in the cytosol of BWM cells and reasoned that release of cytosolic contents from BWM cells would result in detection of YFP fluorescence outside of BWM cells. In BWM cells co-expressing YFP and SNCA::RFP, no extracellular YFP fluorophore was detected and the intensity of YFP fluorescence in BWM cells remained unchanged, while SNCA::RFP was detected in hypodermal tissue (Figure 7A). These results reveal that the intercellular transfer of SNCA::RFP was not a result of membrane leakage.

Recent reports have suggested that overexpression of SNCA can induce the formation of TNTs, membranous protrusions that connect the cytoplasm of remote cells, for the intercellular transfer of various cargo from cell to cell [55]. We therefore examined whether SNCA induces the formation

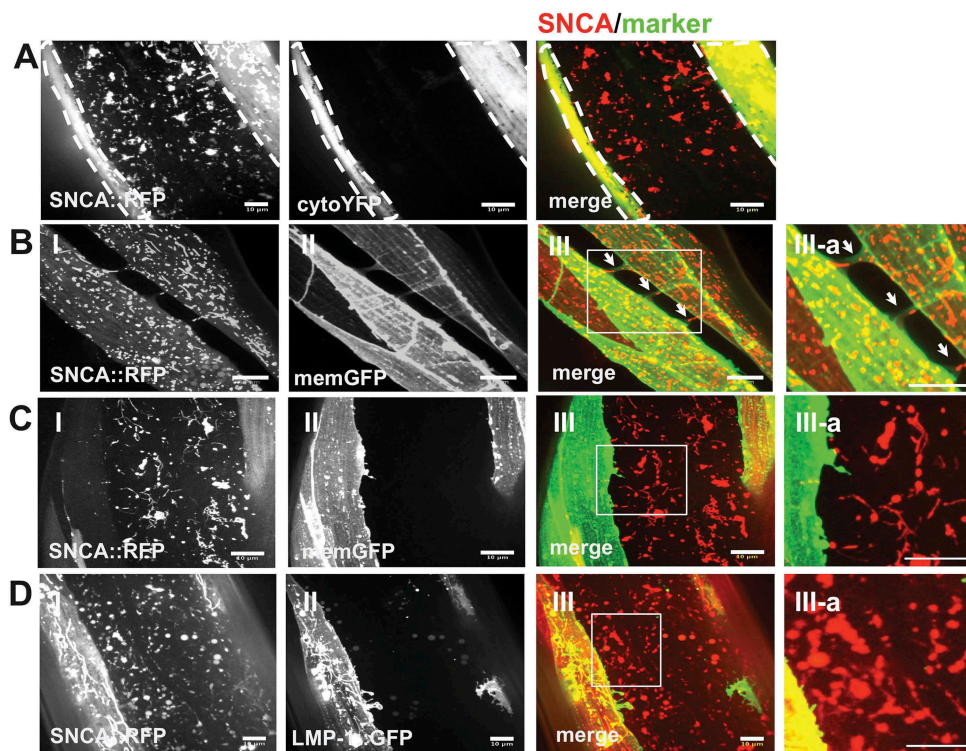


**Figure 7.** SNCA spreading to the hypodermis does not involve transfer of intact endo-lysosomal vesicles through tunneling nanotubes. (A–D) Collapsed confocal z-stacks of 5-d-old nematodes expressing SNCA::RFP together with the indicated markers. (III-a) Zoom of boxed region in (III). Scale bars: 10  $\mu$ m. (A) Release of SNCA::RFP occurs from intact BWM cells. Only SNCA::RFP and not YFP is detected outside BWM cells, indicating that BWM cells are not leaking cytosolic content. (B) SNCA localizes to vesicles within muscle arms that connect BWM cells with motor neuron axons, visualized by the co-expression of membrane anchored GFP in muscle cells. (C) No membrane bound tubes could be detected between muscle cells and hypodermal cells. (D) The lysosomal marker LMP-1 expressed under a BWM cell-specific promoter colocalizes with SNCA vesicles only in BWM cells, whereas SNCA vesicles are detected in BWM and hypodermal cells.

of TNTs for spreading to the hypodermis. Membranous nanotubes were visualized by co-expressing membrane-anchored GFP together with SNCA in BWM cells. While we readily identified as reported 3–4 muscle arms that correspond to specialized membrane extensions, which grow from muscle cells toward motor neurons to form neuromuscular junctions [56] (Figure 7B), we did not observe additional membrane tubes between muscle and hypodermal cells (Figure 7C). However, this level of resolution might be too low to detect very thin tubes. Therefore, we further tested whether intact SNCA containing vesicles might travel from donor to receiving cells. SNCA localizes to endo-lysosomal vesicles in donor and receiving tissues (Figures 2E,F and 4D). If these TNT bridges exist, they would allow the transfer of SNCA together with the surrounding vesicle membrane [55]. In contrast, when the lysosomal membrane marker LMP-1 was co-expressed with SNCA in BWM cells, only SNCA was detected in the hypodermis (Figure 7D). Thus, although SNCA is accumulating within endo-lysosomal vesicles in both donor and receiving tissues, intact SNCA containing organelles are not exchanged. Taken together, these data reveal that neither the uncontrolled release of cytosolic content nor endo-lysosomal trafficking through TNTs seem to play a major role in the transfer of SNCA into epithelial cells.

### Candidate RNAi screen reveals that dissemination of SNCA is mediated by endo- and exocytosis and basement membrane remodeling

Since our results suggest that aggregation and toxicity might affect SNCA spreading, we rationalized that knocking down genes that interfere with SNCA release from BWM cells should increase cell autonomous aggregation and toxicity. Therefore, we tested 110 RNAi clones (Table S2), which were shown to either enhance cell autonomous aggregation or toxicity of SNCA in *C. elegans* [27,29].

Of the 110 genes tested, 17 genes altered the appearance of SNCA::RFP containing vesicles in BWM cells of 5-d-old animals (Figure 8A). We classified the hits into 4 categories: (i) more spherical and fewer tubular vesicles, (ii) more smaller fragmented vesicles, (iii) elongated vesicles, and (iv) highly elongated or connected vesicles (Figure 8A). Of these, 10 also affected inter-tissue transmission and significantly reduced the number of animals in which SNCA::RFP vesicles appeared in the hypodermis (Figure 8B,C). Regarding the phenotypic classes, the 10 final hits distributed as follows: 1 gene of class i, 1 gene of class ii, 5 genes of class iii and 3 genes of class iv, significantly inhibited the transfer of SNCA::RFP (Figure 8A, gene names in bold black letters). Thus, blocking SNCA

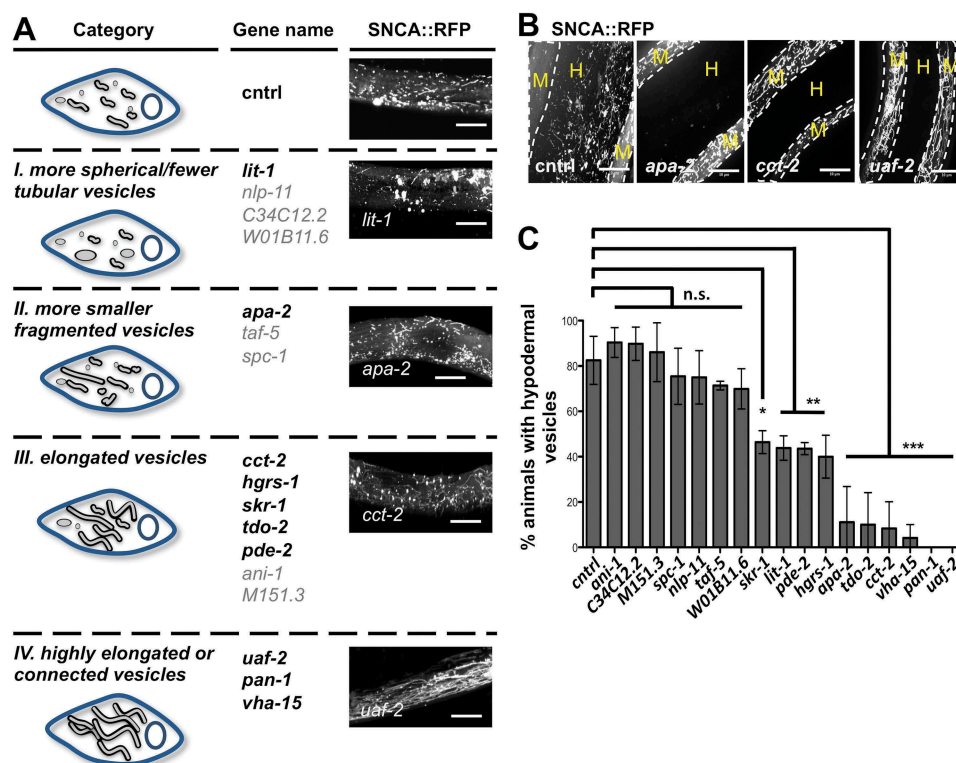


**Figure 8.** Candidate RNAi screen identifies new genetic modifiers of basement membrane transmigration of SNCA. (A) Schematic depiction of the observed vesicle phenotypes in BWM cells in 5-d-old animals. For each category the respective target genes are listed. The effect of one representative gene KD on the appearance of SNCA vesicles is shown on the right (collapsed confocal z-stacks of BWM cells expressing SNCA::RFP). Scale bars: 10  $\mu$ m. (B) Collapsed confocal z-stacks of 5-d-old nematodes expressing SNCA::RFP after KD of the indicated genes. White dashed lines outline the borders of BWM cells. M, muscle; H, hypodermis. Scale bars: 10  $\mu$ m. (C) Quantification of animals that exhibit SNCA vesicles within the hypodermis upon KD of the indicated genes. Data are shown as mean  $\pm$  SEM. Statistical analysis was done using one-way ANOVA with Dunnett's multiple comparison test. n. s. = not significant, \* =  $p < 0.05$ , \*\* =  $p < 0.01$ , \*\*\* =  $p < 0.001$ .

spreading often correlates with an increase of tubular elongated SNCA::RFP containing vesicles in donor BWM cells. However, not all genes that affected the appearance of SNCA::RFP containing vesicles in donor cells impaired spreading of the protein.

While the identified modifiers have diverse functions, the majority of these impacts SNCA dissemination by affecting 2 main biological processes, vesicular transport and basement membrane organization and biogenesis (see also Table S3 for further information on individual hits). Four of the candidate genes function in vesicular trafficking: *cct-2* encodes subunit 2 of chaperonin containing TCP1 (CCT). Depletion of CCT disrupts the microtubule and actin network, impairing intracellular trafficking and lysosomal maturation [57,58], which likely interferes with the trafficking of SNCA::RFP containing vesicles. *hgrs-1* (hepatocyte growth factor-regulated TK substrate [HRS] family; an ESCRT-0 subunit) and *vha-15* (Vacuolar H ATPase) likely interfere with the secretion of SNCA via exosomes [59–61], whereas *apa-2* (adaptin, alpha chain [clathrin associated complex]) might be necessary for the uptake of either free or exosomal SNCA into receiving epithelial cells by clathrin-mediated endocytosis [62].

The second major process that modulates the transfer of SNCA::RFP into the epithelium involves the basement membrane. Half of the identified genetic modulators have a function in ECM remodeling. *skr-1* (SKP1 related [ubiquitin ligase complex component]; ortholog of SKP1) was shown to be required for the expression of a specific set of ECM genes [63], while *pan-1* (P-granule associated novel protein; ortholog of LGR5) and *pde-2* (phosphodiesterase; ortholog of PDE2A, which has a role in tumor growth and invasion [64]) affect ECM composition. LIT-1 (loss of intestine; homolog to human NLK) was recently identified together with CCT as novel regulators of anchor cell invasion through a basement membrane [65], suggesting that a shared set of genes might regulate cell invasion and SNCA spreading.

### SNCA spreads from dopaminergic (DA) neurons to the epithelium

Finally, we asked whether SNCA dissemination to epithelial cells is specific to its expression in muscle cells. We therefore expressed SNCA exclusively in the 8 DA neurons of *C. elegans* (Figure 9A) and monitored the appearance of SNCA in the hypodermis. Besides being visible in DA neuronal bodies and neurites, SNCA was again readily detected in the hypodermis (Figure 9B). Hence, the transfer of SNCA into the hypodermis is not limited to an expression in BWM cells. While the onset of DA to hypodermis transmission was still age-dependent, it occurred during development in 3-d-old animals (L4s) (Figure 9C), a much earlier stage compared to the onset observed for BWM to hypodermis transmission, suggesting that DA neurons might be more vulnerable to the accumulation of SNCA. Moreover, the basement membrane might constitute an additional barrier for SNCA spreading. Neurons of the somatic nervous system (including DA neurons) share a basement membrane with the hypodermis that isolates them from other tissues, such as the body wall muscle tissue. Since there is no basement membrane between neurons

and the hypodermis, the intercellular transmission of SNCA should not be affected by the knockdown of genes involved in basement membrane remodeling. In line with this, only genes that are involved in vesicle trafficking affected the spreading of SNCA in these animals (Figure 9D,E). Hence, the dissemination of SNCA across an interstitial ECM depends mainly on vesicle transport processes, while systemic spreading across the more complex ECM of a basement membrane relies on additional changes that only occur later in life.

Reduced INS-IGF1 signaling in *daf-2* mutants resulted in only a minor improvement in morphological abnormalities observed in CEP neurons expressing SNCA::RFP (Figure 9F and S7A), but a significant reduction in neurodegeneration on day 6 in a partially *daf-16* dependent manner (Figure 9G), consistent with previous *daf* reports [66]. The SNCA;*daf-2* mutant animals also tended to perform better than SNCA WT nematodes in a basal slowing response assay that reflects DA function (Figure S7B and S7C). Moreover, the transmission of SNCA::RFP was delayed in the *daf-2* mutant background in a *daf-16* dependent manner (Figure 9H), in accordance with its effect on SNCA::RFP expressed in BWM cells.

The sfGFP::LGALS3 reporter revealed that the continuous spreading of SNCA from DA neurons into hypodermal cells caused again endo-lysosomal rupture, which was almost completely suppressed in *daf-2* mutant animals (Figure 9I,K). These results confirm that reducing INS-IGF1 signaling protects endo-lysosomal vesicles against proteotoxic damage.

## Discussion

We describe a new SNCA/ $\alpha$ -synuclein animal model that facilitates non-invasive tracking of a fraction of SNCA, which accumulates in endo-lysosomal vesicles during aging. Accumulated SNCA conformers are transferred from expressing muscle cells or DA neurons to the epithelial tissue of *C. elegans*. Our genetic and cell biological evidence supports a model (Figure S8), in which SNCA is transferred from tissue to tissue via vesicular endo- and exocytosis rather than via passive diffusion or tunneling nanotubes. Moreover, the transfer of SNCA across a basement membrane required additional alterations in ECM composition that occurred at later ages. Finally, the accumulation of SNCA in endo-lysosomal vesicles in receiving epithelial cells resulted in non-cell autonomous toxicity by endo-lysosomal membrane permeabilization (LMP), which could be prevented by reducing INS-IGF1 signaling.

SNCA containing vesicles colocalize with lysosomal markers but have morphological characteristics and properties that are distinct from classical mature lysosomes. Intriguingly, similar lysosomal shapes and dynamics were recently described upon overexpression of the amino acid transporters CTNS-1 and LAAT-1 [67]. The over-expression of certain amino acid transporters, as well as the accumulation of SNCA, is known to impair lysosomal homeostasis [34,68,69]. Consistent with this, co-expression of SNCA and CTNS-1 had a synergistic effect and enhanced vesicle tubulation (Figures 2F and 4D), whereas impaired INS-IGF1 signaling reduced the number of tubular vesicles (Figure 5C). This suggests that the observed vesicular structures and dynamics



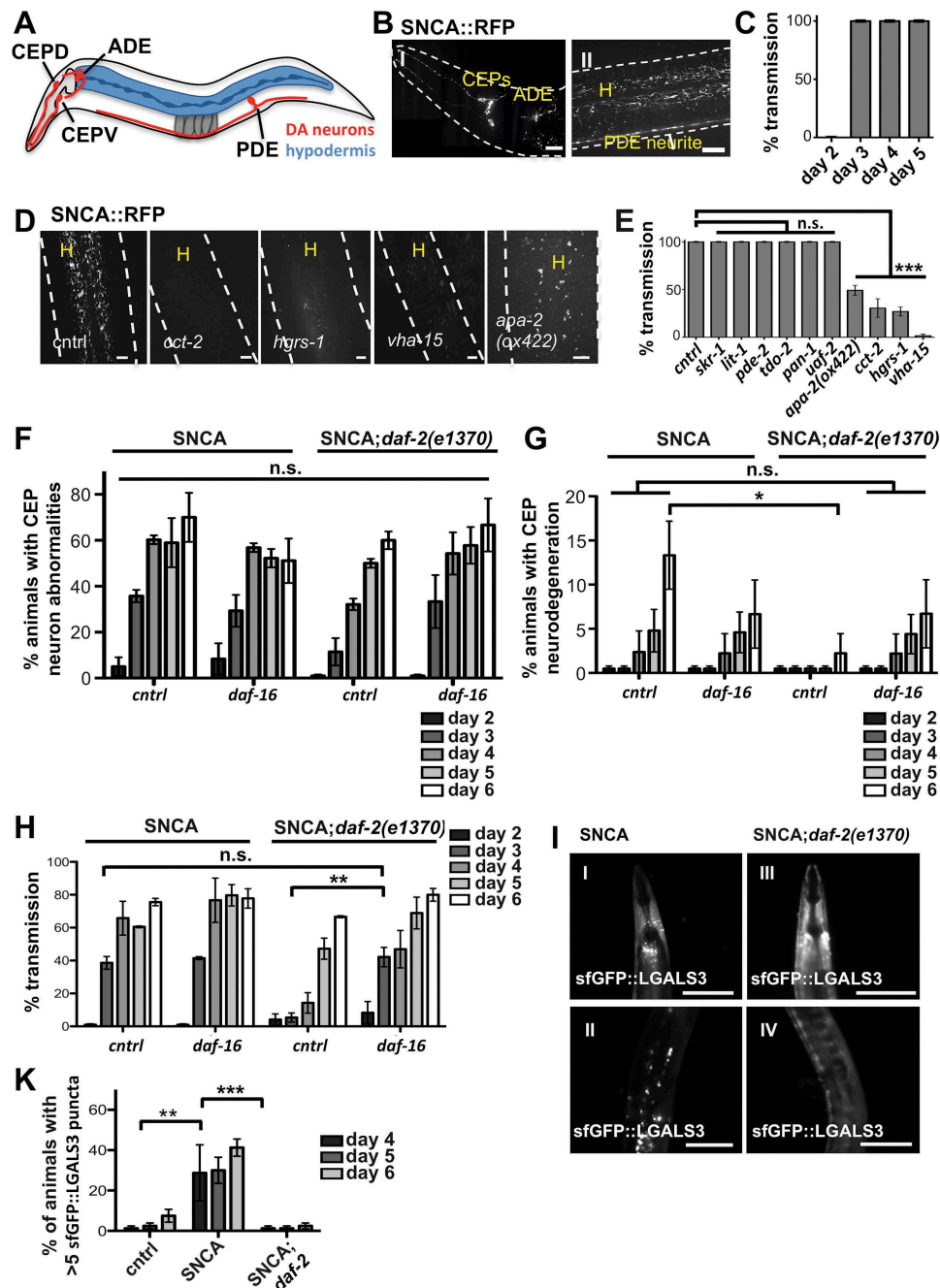


**Figure 9.** Spreading of SNCA from DA neurons to the hypodermis is modulated by genes involved in vesicular trafficking and results in endo-lysosomal rupture that is suppressed by reduced INS-IGF1 signaling. (A) Schematic depiction of the 8 DA neurons of the *C. elegans* hermaphrodite, which include 4 bilaterally symmetric pairs of neurons (only one side is depicted): 2 pairs of cephalic neurons (2 dorsal CEP [CEPD] and 2 ventral CEP [CEPV]), one pair of anterior deirid sensillum (ADE), and one pair of posterior deirid neurons (PDE). (B,D) Collapsed confocal z-stacks of nematodes expressing SNCA::RFP in DA neurons under the DA transporter promoter (*dat-1p*). White dashed lines outline the borders of animals. H: hypodermis. Scale bars: 10  $\mu$ m. (B) SNCA::RFP fluorescence is detected in DA neurons (I) and in the hypodermis (II) in 5-d-old animals. I: 3 different images were stitched together to create a high-resolution montage of the head region. CEP: cephalic neuron, ADE: anterior deirid neuron. (C) Quantification of SNCA::RFP transmission into the hypodermis at indicated ages. (D) Images of 3-d-old nematodes expressing SNCA::RFP in DA neurons after KD of the indicated genes or harboring the indicated mutation. In 49% of SNCA::RFP;*apa-2(ox422)* animals in which hypodermal vesicles were detected, the vesicles were fewer and appeared round and not tubular shaped, indicating that endocytic vesicles did not further mature into lysosomes. (E) Quantification of SNCA::RFP transmission into the hypodermis in 3-d-old animals upon KD of the indicated genes or harboring the indicated mutation. (F) Quantification of SNCA::RFP expressing animals that exhibit strong morphological abnormalities of CEP neuron axons and dendrites at indicated ages in the WT and *daf-2* mutant background and upon KD of the indicated genes. (G) Quantification of SNCA::RFP expressing animals exhibiting a loss of at least one CEP neuron at indicated ages in the WT and *daf-2* mutant background and upon KD of the indicated genes. (H) Quantification of SNCA::RFP transmission at indicated ages in the WT and *daf-2* mutant background and upon KD of the indicated genes. KD of *daf-16* abolishes the *daf-2*-mediated suppression of SNCA::RFP spreading on day 3. (I) Collapsed z-stacks of the hypodermis of 5-d-old nematodes. sfGFP::LGALS3 puncta reveal endo-lysosomal leakage in hypodermal cells when SNCA::RFP is expressed in DA neurons in WT animals (I: head region and II: periphery), but not in animals harboring the *daf-2* mutation (III: head region and IV: periphery). Scale bars: 100  $\mu$ m. (K) Quantification of animals with more than 5 sfGFP::LGALS3 foci at indicated ages. Data information: In (C,E–H) data are shown as mean  $\pm$  SEM. In (K) data are shown as mean  $\pm$  SD. In (E) statistical analysis was done using one-way ANOVA with Dunnett's multiple comparison test. In (F–H,K) statistical analyses were done using two-way ANOVA with Bonferroni posttests. n. s. = not significant, \* =  $p < 0.05$ , \*\* =  $p < 0.01$ , \*\*\* =  $p < 0.001$ .

could result from endo-lysosomal stress and may represent pre-lysosomal compartments destined for secretion [70].

*C. elegans* has been instrumental in discovering genes that link vesicular trafficking and lysosomal function to SNCA neurotoxicity or spreading, which have been successfully translated to higher eukaryotes [71–74]. Furthermore, a number of studies in mammalian cell culture models suggested that SNCA is transferred by vesicular exo- and endocytosis, and secreted by an unconventional, endoplasmic reticulum/Golgi-independent exocytosis [46,75–77]. In addition, the interplay between proteotoxic stress, (impaired) SNCA clearance and spreading pathways is becoming increasingly clear [34,46,47,49,76]. Thus, multiple aspects of our findings resemble observations in mammalian models and patients, underlining the relevance of our results for understanding the pathology of the human disease.

This study revealed that accumulation of SNCA in endo-lysosomal vesicles of post-mitotic cells such as muscles or DA neurons leads to the transmission of the protein into neighboring epithelial cells for remote degradation, suggesting that the degradation of lysosomal content is coordinated across tissues of a multicellular organism. Our results indicate that failure of lysosomal degradation in one tissue leads to the transfer of hardly digestible substrates to neighboring epithelial cells. A recent transcriptome analysis of *C. elegans* identified the hypodermis as a tissue with major metabolic and immune functions with a transcriptional profile showing significant similarities with human liver and blood plasma as well as immune cells [78]. It is therefore tempting to speculate that the transfer of SNCA might be either part of a detoxification pathway, a metabolite-recycling pathway or an organismal immune surveillance pathway.

A similar pathway for the removal of cellular debris has been recently described: *C. elegans* neurons were shown to expel misfolded proteins within exophers, large membrane-surrounded vesicles containing damaged cytoplasmic material [25]. While the timing is similar, there are 2 lines of evidence that do not support a major role of exophers in SNCA spreading observed here. First, exopher content was shown to be phagocytosed by the hypodermis [25]. If transfer of SNCA involved phagocytosis, it should not be affected by *apa-2* depletion, since knockdown of *apa-2* in *C. elegans* does not inhibit phagocytosis by the hypodermis [79]. The uptake of SNCA into the epithelium likely involves clathrin-mediated endocytosis. Second, SNCA spreading is very efficient occurring in ~70–100% of animals once initiated, whereas exopher release was observed in ~10% of animals. Since we occasionally did observe exophers in our imaging analysis that seemed to originate from SNCA::RFP expressing cells, exopher-mediated transfer might occur in parallel to the transfer by exo- and endocytosis and could account for the ~10% of transmission that we also detected with other aggregation-prone proteins (Figure S4). However, more experiments would be required to examine the exact pathways and the potential involvement of exophers.

This inter-tissue dissemination of SNCA is strikingly age-dependent. While the spreading from DA neurons to hypodermis occurs during development between the second and fourth larval stage (corresponding to 2- and 3-d-old animals),

the transmigration across a basement membrane occurs between day 1 to day 2 of adulthood (corresponding to 4- and 5-d-old animals). Intriguingly, the latter coincides with a decline of the functional capacity of the proteostasis network, which undergoes drastic changes at that age [1,80,81]. Moreover, there is increasing evidence that organismal proteostasis, the cytoskeleton and ECM homeostasis are interdependent [82,83]. Our data revealed that remodeling of the basement membrane was essential for SNCA spreading from BWM cells to the hypodermis, which is supported by the identification of several modifiers that function in cell invasion and cancer progression. Furthermore, lysosomal exocytosis might also increase the dissemination of SNCA across the basement membrane, since the secretion of lysosomal content also mediates ECM degradation in cell invasion during normal development or cancer metastasis [84,85]. This suggests that the transfer of a protein across a basement membrane might share molecular mechanisms with the transmigration of an entire cell.

A surprisingly small number of candidates (only 10 out of 110) inhibited SNCA spreading, although our results with SNCA<sup>A53T</sup> and *daf-2* mutant animals suggested that spreading is influenced by aggregation and toxicity. Moreover, there was no clear correlation between genes regulating SNCA spreading and genes regulating its aggregation and/or toxicity: 4 of the 10 hits that reduce spreading had been previously identified to increase SNCA inclusion formation upon knockdown (*tdo-2*, *hgrs-1*, *vha-15* and *uaf-2*), whereas knockdown of 6 genes have been shown to enhance SNCA toxicity (*apa-2*, *pde-2*, *lit-1*, *skr-1*, *cct-2*, and *pan-1*) [27,29]. There is increasing evidence that aggregation and toxicity are uncoupled, as the formation of large visible protein aggregates might even be protective under certain circumstances [86,87]. The absence of a clear correlation suggests that spreading represents another distinct trait of SNCA pathology. Hence, aggregation, toxicity and spreading, though affecting each other, seem to be regulated by several distinct pathways and component genes that may or may not interact.

The identified modifiers could affect systemic SNCA::RFP spreading by multiple means. *apa-2*, *hgrs-1*, *vha-15* and *cct-2* likely regulate vesicular trafficking of SNCA::RFP. *cct-2* encodes subunit 2 of chaperonin-containing TCPI (CCT), which has a well-characterized role in tubulin and actin folding. Depletion of this complex disrupts the microtubule and actin network and impairs intracellular trafficking [57]. Moreover, CCT knockdown affects autophagy and lysosomal function [58]. Thus, reducing the levels of CCT-2 likely interferes with the trafficking of secretory SNCA::RFP containing vesicles. *hgrs-1* encodes hepatocyte growth factor-regulated tyrosine kinase substrate (HGS), an ESCRT-0 protein. Besides being involved in the generation of MVBs by sorting ubiquitinated proteins into intraluminal vesicles of MVBs and targeting it to lysosomal degradation, HGS was shown to regulate exosome secretion in dendritic cells [61] and could therefore affect the spreading of SNCA by exosomes. Moreover, ESCRT-0 has a role in sorting ubiquitinated cargo for lysosomal degradation at the plasma membrane, consistent with a role in uptake of SNCA in receiving tissues [88]. *vha-15* encodes the regulatory subunit H of the

peripheral H<sup>+</sup>-transporting V<sub>1</sub> complex of the vacuolar ATPase (V-ATPase), which functions in endosome acidification and maturation. This activity could be necessary for the maturation of SNCA-containing endosomes and subsequent release from donor cells. Additionally, *vha-5*, encoding a subunit of the membrane-bound V<sub>0</sub> domain of the V-ATPase mediates exosomal release from the *C. elegans* hypodermis [59], independent of its contribution to the proton pump activity. Because the V<sub>0</sub> domain can be directly involved in both budding and fusion events of secretory vesicles [60], the KD of *vha-15* might also interfere with SNCA spreading by affecting the function of the V<sub>0</sub> domain. Finally, *apa-2* encodes the  $\alpha$ -adaptin subunit of the AP2 complex in clathrin-mediated endocytosis (AP2A1), and is likely necessary for the endocytic uptake of either free or exosomal SNCA into receiving epithelial cells.

Half of the genetic modulators identified have a function in ECM remodeling. For example, *skr-1* encodes an ortholog of SKP1 (S-phase kinase associated protein 1), an essential component of the SCF (SKP1-CUL1-F-box protein) ubiquitin ligase complex, and is required for the expression of a specific set of ECM genes [63]. *pan-1* is an extracellular leucine-rich repeat protein, orthologous to LGR5 (leucine rich repeat containing G protein-coupled receptor 5) with a role in molting [89], for which it is tempting to speculate that *pan-1* RNAi might prevent the formation of ECM structures that allow transmission of SNCA. *pde-2* is an ortholog of PDE2A/cGMP-dependent 3',5'-cyclic phosphodiesterase that has a role in tumor growth and invasion [64] and could also affect ECM composition. LIT-1 is a serine/threonine-protein kinase homolog related to human NLK (nemo like kinase). LIT-1 was recently identified together with CCT as novel regulators of anchor cell invasion through a basement membrane [65], suggesting that a shared set of genes might regulate cell invasion and SNCA spreading.

The following 2 candidates do not fall into the categories mentioned above. *uaf-2* codes for an essential U2AF1/splicing factor U2AF 35 kDa subunit homolog and plays a critical role in alternative splicing of various proteins. Whether its role in splicing or whether the early developmental arrest caused by its depletion prevents spreading of SNCA needs to be established in future studies.

Depletion of *tdo-2*, an ortholog of human TDO2 (tryptophan 2,3-dioxygenase), was recently shown to suppress aggregation and toxicity of SNCA in *C. elegans* [90]. Perturbations in the kynurenine pathway of tryptophan degradation have been implicated in aging as well as the pathogenesis of many age-related diseases [91]. However, the mechanism by which the inhibition of *tdo-2* expression protects against SNCA spreading warrants further investigation.

Taken together, some of the genes identified in our candidate screen may become promising candidates for targets of intervention in synucleinopathies. Still, further studies are necessary to explore their therapeutic value.

Although it is well established that SNCA exhibits non-cell autonomous toxicity [7,8], the underlying mechanisms remain elusive. A distinct advantage of our *C. elegans* model is the ability to simultaneously but separately monitor the dynamics of SNCA containing vesicles, in both donor and

receiving tissues. Other systems such as the bimolecular fluorescence complementation (BIFC)-based models express SNCA in both, donor and receiving cell populations, and transmission occurs bi-directionally, thus preventing an ability to distinguish between cell autonomous and non-cell autonomous effects [92,93]. Here we show that intercellular transmission of SNCA expressed in neighboring tissue is sufficient to provoke non-cell autonomous toxicity by inducing endocytic vesicle rupture. Endo-lysosomal membrane permeabilization (LMP) is toxic and causes mitochondrial damage, reactive oxygen species production and can ultimately trigger cell death [52,94]. Such chronic detrimental interactions between secreted pathological proteins and epithelial cells might eventually lead to epithelial cell dysfunction. This might facilitate invasion of misfolded SNCA from peripheral tissues and the circulatory system into the CNS [95]. Furthermore, the chronic transfer from neurons to the epithelial layer might lead to blood-brain-barrier breakdown, which is frequently observed in PD and other neurological disorders [96,97]. Blood-brain-barrier leakage might contribute to neurodegeneration as it often results in decreased efflux and subsequent accumulation of toxic molecules including SNCA [95,96]. Thus, continuous spreading and accumulation of misfolded SNCA appears to interfere with the function of multiple cell types and tissues without the manifestation of characteristic SNCA inclusions.

Aging is a major risk factor for the development of PD and reducing INS-IGF1 signaling has been shown to protect against SNCA associated neurodegeneration [66,98]. Our study provides further mechanistic details by showing that impaired DAF-2 function prevents vesicle rupture caused by the accumulation of toxic SNCA conformers. This is consistent with recent work showing that inhibition of INS-IGF1 signaling suppresses lysosomal damage and rescues lifespan of *scav-3* (scavenger receptor [CD36 family] related; human SCARB2 homolog) mutant animals [67]. Our results provide further evidence that preserving endo-lysosomal integrity is essential to maintain cellular homeostasis during aging and proteotoxic stress. Since endo-lysosomal dysfunction is emerging as key pathological event in various neurodegenerative disorders [99–101], preventing LMP might constitute an effective therapeutic strategy.

## Materials and methods

### Maintenance of *C. elegans* and age-synchronization

Wild type (WT) Bristol N2, as well as transgenic animals, were cultured using standard methods [102]. If not otherwise indicated, worms were grown on nematode growth medium (NGM; 50 mM NaCl [Labochem international, LC-5932.1], 0.25 w:v Bacto-Peptone [BD Biosciences, 211820], 1.8% Bacto-Agar [BD Biosciences, 214030], 1 mM MgSO<sub>4</sub> [Carl Roth, P027.3], 1 mM KH<sub>2</sub>PO<sub>4</sub>, pH = 6 [Serva Electrophoresis GmbH, 26780.01], 1 mM CaCl<sub>2</sub> [Carl Roth, T885.1], 5  $\mu$ g/ml Cholesterol [Sigma-Aldrich, C8667] in EtOH) plates seeded with *E. coli* strain OP50 (*Caenorhabditis* Genetics Center, OP50) at 20°C. Animals were age-synchronized by bleaching [103]. Shortly, gravid adults were dissolved in alkaline hypochlorite solution (250 mM NaOH



[Carl Roth, P031.2] and 20% sodium hypochlorite solution [NaOCl, min. 14% free chlorine; Thermo Fisher Scientific, 10691164] in H<sub>2</sub>O). The remaining *C. elegans* embryos were washed 2 times with M9 buffer (21 mM Na<sub>2</sub>HPO<sub>4</sub> [Sigma-Aldrich, 30414], 22 mM KH<sub>2</sub>PO<sub>4</sub>, 85 mM NaCl, 1 mM MgSO<sub>4</sub>) and let hatch with gentle rocking in M9 buffer at 20°C overnight. The next day, L1 larvae were distributed onto NGM or RNAi plates (NGM medium supplemented with 100 µg/ml Ampicillin [Carl Roth, K029.2], 12.5 µg/ml Tetracycline [Sigma-Aldrich, T3383], 1 mM IPTG [Carl Roth, 2316.4]), seeded with the respective bacteria and grown at 20°C. Animals reached day 2 of adulthood 4 d later (corresponding to 5-d-old animals). Alternatively, nematodes were age-synchronization by egg laying [36], by allowing adult animals to lay eggs for 2–3 h before removing them again from the plates. Embryos were grown at 20°C and assayed at the indicated days of life.

### Cloning of *C. elegans* expression constructs and generation of transgenic animals

For constructing *C. elegans* expression constructs, the MultiSite Gateway Three-Fragment Vector Construction Kit (Thermo Fisher Scientific, 12537-103) was used. The cDNA of WT human SNCA was amplified from a pPD30.38 (Addgene, 1443) expression vector [27] by PCR using oligonucleotides suitable for gateway cloning and inserted into the pDONR221 (Thermo Fisher Scientific, 12537-103) entry vector by recombination. The entry vector coding for A53T mutant human SNCA (SNCA<sup>A53T</sup>) was generated by mutagenesis PCR using the pDONR221 vectors as a template. Entry vectors pDONR P4-P1R (Thermo Fisher Scientific, 12537-103) containing the *myo-3* promoter region (approx. 2.4 kb upstream of the *myo-3* gene), or the *unc-54* promoter region (approx. 1 kb upstream of the *unc-54* gene) and pDONR P2R-P3 (Thermo Fisher Scientific, 12537-103) coding for the C-terminal monomeric RFP tag and the *unc-54* 3'UTR, were generated previously [36]. The entry vector pDONR P4-P1R containing the *dat-1* promoter region (approx. 1.4 kb upstream of the *dat-1* gene) was purchased (Dharmacon, PCE1182-202307362). The pDONR221 entry vector coding for sfGFP::Gal3 was generated by amplifying the cDNA of sfGFP::Gal3 from a pPD49.26 (Addgene, 1686) expression vector [53]. The Y37A1B.5 promoter region (approx. 2.9 kb upstream of the Y37A1B.5 gene) was amplified from a *C. elegans* lysate and recombined into the pDONR P4-P1R vector to mediate hypodermis-specific expression. Entry vectors containing the respective promoters, cDNAs and 3'UTRs were inserted into the destination vector pDEST R4-R3 (Thermo Fisher Scientific, 12537-103) in an *in vitro* recombination reaction to create the *myo-3p::SNCA WT::rfp::unc-54 3'utr*, *myo-3p::SNCA<sup>A53T</sup>::rfp::unc-54 3'utr*, *dat-1p::SNCA WT::rfp::unc-54 3'utr*, and *unc-54p::sfGFP::LGALS3::unc-54 3'utr* expression constructs.

The plasmids were injected into young adult N2 hermaphrodites to generate transgenic lines carrying an extrachromosomal array. Some plasmids were subsequently integrated by gamma irradiation (*myo-3p::WT SNCA* and *SNCA<sup>A53T</sup>*) or UV irradiation (*dat-1p::WT SNCA*). Successfully integrated lines were backcrossed at least 5 times into the WT N2 background. Strains used in this study are listed in Table S1.

### Drug treatments

Transgenic *C. elegans* expressing SNCA::RFP in the *bus-17* (*e2800*) mutant background were used in these experiments. The impermeability of the adult *C. elegans* cuticle necessitated the use of the *bus-17* mutation for acute drug treatments [45,104]. 5-d-old animals were washed off from regular NGM plates with M9 and incubated for 30 min in M9 buffer containing either 2% DMSO (Sigma-Aldrich, 276,855) as control, or 2% DMSO plus 100 µM nocodazole (NOC; Sigma-Aldrich, M1404), or 2% DMSO plus 10 mM sodium azide (NaN<sub>3</sub>; Carl Roth, K305.1). Immediately after treatment, animals were mounted on microscope slides for imaging as detailed below. Unfortunately, due to deleterious side effects these drugs could only be administered for a short period of time (up to 1 h), which renders it impossible to test whether the disruption of the microtubule network in donor cells would also completely block the intercellular transfer of SNCA.

### Fluorescence microscopy

For imaging, age-synchronized animals were mounted on 5–10% agarose (VWR Chemicals, 35–1020) pads and immobilized in a solution containing 2.5 mM levamisole (Applichem, A4341) and nanosphere size standards (100 nm polystyrene beads, Thermo Fisher Scientific, 3100A). Colocalization of SNCA::RFP with individual markers was examined with a Zeiss LSM 780 confocal microscope (Zeiss, Germany) equipped with a 488 nm Argon laser (25 mW) and a 561 nm DPSS laser (20 mW), and Zeiss ZEN 2010 software (Figures 2B–2F, 3A, 6A, 7A,B and 8A). Z-stack (0.2 µm steps) or time-lapse (1–2 frames per second [fps]) images were acquired for each channel using a Plan-Apochromat 63x/1.4 oil objective. This system allows free selection of the spectral detection range, which was flexibly adapted to ensure full separation of fluorescent signals for each combination of fluorophore. Colocalization of SNCA::RFP with each of the vesicle markers was quantified by the colocalization function of Zeiss ZEN software. For each condition, at least 20 images were measured to calculate the colocalization coefficients for the RFP channel (by summing the pixels in the colocalized region divided by the sum of pixels in the RFP channel).

High sensitivity microscopy was performed using a Leica DMI8SD AF spinning disc microscope (Leica Microsystems, Germany) equipped with a 561 nm diode laser (50 mW) and the MetaMorph Advanced Acquisition software (Molecular Devices, U.S.A.) (Figure 1A,B; 4(b); 4f; 5a; 6c; 8b; 9b; 9d; S1c and S1d; S2; S7; Videos S1 and S6). Z-stacks (0.2 µm steps) or time-lapse (1–2 fps) images were acquired for each channel using an Orca Flash 4.0 LT (C11440-42U) camera (Hamamatsu, Japan) and a HC PL APO 40x/1.3 oil or 63x/1.40–0.60 oil objective. High sensitivity combined with colocalization microscopy was performed using a PerkinElmer ERS-VoX spinning disk confocal microscope (PerkinElmer, U.S.A.) on a Nikon Eclipse Ti-E microscope (Nikon, Japan) (Figures 4C,D and 7C,D; S4; Video S2), which was equipped with lasers of 488 and 561 wavelength for fluorochrome excitation and green (527/55) and red (615/70) band pass filters for detection of fluorochrome emission. Z-stacks

(0.2  $\mu\text{m}$  steps) or time-lapse (1–2 fps) images were recorded with a Hamamatsu C9100-02 EMCCD camera (Hamamatsu, Japan) using a Nikon Plan Apo VC 60x NA 1.2 water immersion objective (Nikon, Japan). For Figures 3B, 6E and 9I; and Videos S3–S5, a widefield imaging system (excellence IX81, Olympus, Japan) equipped with an UPlanSApo 40x/0.95 and an Apo N 60x/1.49 oil objective was employed. Z-stacks (0.2  $\mu\text{m}$  steps) or time-lapse (1–2 fps) images were recorded with an Orca-R2 EMCCD camera (Hamamatsu, Japan) using excellence software (Olympus, Japan). For Figure S6 a Leica M205 FA microscope with a Leica DFC310FX camera and the Leica DFC Twain Software were used (Leica Microsystems, Germany). All further processing of acquired images was performed with ImageJ software (NIH). If not otherwise indicated, maximum projections of z-stacks are shown. The PureDenoise plugin (<http://bigwww.epfl.ch/algorithms/denoise/#ij>, EPFL) for ImageJ was used to denoise videos where indicated in the video legend [105].

### Fluorescence lifetime imaging microscopy (FLIM)

SNCA::RFP, SNCA::RFP;*daf-2* or RFP expressing nematodes were analyzed by FLIM on days 4, 5, 6 and 10 of life as previously described [37]. Briefly, nematodes were anesthetized with 250 mM  $\text{NaN}_3$  for up to 30 min, mounted on a 2.5% agarose-pad for subsequent confocal microscopy and fluorescence lifetime measurements. Measurements were performed using a SP5 (Leica Microsystems, Germany) confocal microscope, objectives used were HCX PL APO 63  $\times$  1.2 and HCX PL APO CS 100  $\times$  1.4. The applied zoom was up to 2-fold. Images were recorded by time correlated single photon counting (TCSPC) using PicoHarp 300 (PicoQuant, Germany). A pulsed supercontinuum laser was used for excitation, emitting pulses at 80 MHz. An acousto-optic beam splitter was used to set the excitation light to 587 nm and to measure emission between 590–700 nm. Photon counting rates were kept below 1% of the laser repetition rate to prevent photon pileup. Images were acquired until 1,000–2,000 photons per pixel were recorded. Images were processed with Flimfit software [106] and fitted as mono-exponential decays. Further analysis was done with OriginPro 9.0 (OriginLab, U.S.A.) and Excel 2016 (Microsoft, U.S.A.).

### Correlative light and electron microscopy (CLEM)

#### High pressure freezing (HPF)

Age-synchronized 5-d-old animals, grown on HT115 (DE3) (Source Bioscience, 3318\_Cel\_RNAi\_complete) or OP50 *E. coli* bacteria, were picked individually and transferred to 0.1 mm deep aluminium carriers (Engineering Office M. Wohlwend GmbH, 241), filled with a paste of OP50 bacteria mixed with 10% bovine serum albumin (BSA [Biowest, P6154]) in  $\text{H}_2\text{O}$ . The samples were covered with an additional aluminium carrier and high pressure frozen using the HPM010 high pressure freezer (Bal-Tec, Liechtenstein).

#### Freeze substitution and CLEM

Freeze substitution was done using a freeze substitution device EM-AFS2 (Leica Microsystems, Austria). The freeze

substitution solution for CLEM contained 0.1% (w/v) uranyl acetate (Science Services, 22,400) in dry acetone (Applichem, 131,007.1611) and the samples were substituted at  $-90^\circ\text{C}$  for 48 h. The temperature was then increased at a rate of  $5^\circ\text{C}/\text{h}$  to  $-45^\circ\text{C}$  followed by 5 h incubation at  $-45^\circ\text{C}$ . Samples were rinsed with acetone followed by step wise (10%, 25%, 50%, 75%, 4 h each) lowicryl HM20 (Polysciences, 15,924–1) infiltration at  $-45^\circ\text{C}$  to  $-25^\circ\text{C}$ . 100% lowicryl was exchanged 3 times every 10 h. UV polymerization was applied for 48 h at  $-25^\circ\text{C}$  and the temperature was increased to  $20^\circ\text{C}$  at a rate of  $5^\circ\text{C}/\text{h}$ . Finally the samples were left exposed to UV at room temperature for 24 h.

Sectioning was done on a Leica UC6 ultramicrotome (Leica Microsystems, Austria) and sections were collected on carbon coated 200 mesh copper grids (Electron Microscopy Sciences, U.S.A., CF200-Cu). Grids with 90-nm thick sections were placed on a drop of water and sandwiched between 2 cover-glasses and imaged with sections facing the objective by fluorescent light imaging using a Leica DMI8SD AF spinning disc microscope (Leica Microsystems, Germany) equipped with a 561 nm diode laser (50 mW) and the MetaMorph Advanced Acquisition software. Single plane images were acquired using a Hamamatsu Orca Flash 4.0 LT camera (Hamamatsu, Japan, C11440-42U) and a HC PL APO 100x/1.4 oil CS2 objective. Subsequently, grids were stained with 3% uranyl acetate and Reynold's lead citrate (0.08 M Lead[II]-nitrate [Carl Roth, HN32.1] and 0.16 M Trisodium citrate dehydrate [Sigma-Aldrich, S1804]) and the identical areas, identified by position on the grid in relation to grid centre, were imaged on a JEOL JEM-1400 electron microscope (JEOL, Japan) operating at 80 kV and equipped with a 4K TemCam F416 (Tietz Video and Image Processing Systems GmbH, Germany). In the final step the correlation of fluorescence and electron micrographs, based on morphological features, was done using the eC-CLEM software [107].

#### Freeze substitution and TEM for ultrastructure

In addition, some high-pressure frozen samples were processed for morphological studies. The freeze substitution solution did in this case consist of 2% osmium (Science Services, 19,110), 0.5% uranyl acetate and 3% water in dry acetone. The substitution was done at  $-90^\circ\text{C}$  for 35 h, followed by warming at  $5^\circ\text{C}/\text{h}$  to  $-60^\circ\text{C}$ . The samples were incubated at this temperature for 4 h, warmed to  $-30^\circ\text{C}$  and incubated for 8 h before the temperature was increased to room temperature. The samples were rinsed in dry acetone, infiltrated step wise (30%, 60%, 100%) in Spurr's resin (45 g ERL-4221D [Serva Electrophoresis GmbH, 21,041.02], 27 g D.E.R.736 [Serva Electrophoresis GmbH, 18,247.01], 117 g NSA [Serva Electrophoresis GmbH, 30,812.01], 1.8 g DMAE [Serva Electrophoresis GmbH, 20,130.02]) and polymerized at  $60^\circ\text{C}$ . 70 nm thin sections of these samples were collected on formvar (Science Services, 15,800) coated copper slot grids (Plano, G 2500C). Post stained sections were imaged as described above.

#### Worm lysis, western blot and signal quantification

Nematodes were washed 2 times in M9 buffer, and then in lysis buffer (20 mM Tris, pH 7.5 [Carl Roth, 4855.2]; 10 mM

$\beta$ -mercaptoethanol [Sigma-Aldrich, M3148]; 1% Triton X-100 [Merck, 1.08643.1000]; supplemented with complete protease inhibitor cocktail [Roche, 05056489001]) before shock freezing in liquid nitrogen. Equal volumes of lysis buffer were added along with an appropriate amount of zirconia beads (0.7 mm, BioSpec Products; Carl Roth, N037.1). Worms were mechanically lysed using a FastPrep-24 homogenizer (MP Biomedicals, Germany; 6.5 m/s, 60 s at 4°C). The lysates were transferred into fresh Eppendorf tubes to remove beads and centrifuged (100 x g for 2 min at 4°C) in a tabletop centrifuge to remove carcasses. The supernatant was transferred into fresh Eppendorf tubes and protein concentration was determined using protein assay dye reagent concentrate (Bio-Rad, 500-006). Proteins were separated under denaturing conditions by SDS-PAGE and transferred onto a PVDF membrane (Carl Roth, T830.1) by semi-dry or wet blotting using standard protocols. For transgene detection, mouse monoclonal anti-SNCA antibody (211, Santa Cruz Biotechnology, sc-12767) or anti-mCherry antibody (1C51, Abcam, ab125096) were used. Anti-actin antibody (clone C4, Sigma-Aldrich, MAB1501) was used as loading control. Alkaline phosphatase (AP)-conjugated anti-mouse IgG secondary antibodies (Vector Laboratories, AP-2000) were used for subsequent ECF-based detection (GE Healthcare, RPN5785). Western blot signal intensity analysis was performed using the gel analyzer function of ImageJ on results from 3 independent experiments.

### Sequential extraction of SNCA

Detergent fractionation of worm lysates was performed according to the procedure described in Kuwahara et al. [39] with minor modifications. Nematodes were washed 2 times in M9 buffer, and once in Tris-HCl buffer (50 mM Tris, pH 7.5, supplemented with complete protease inhibitor cocktail [Roche, 05056489001]), shock frozen in liquid nitrogen and kept at -80°C. The worm pellet was re-suspended in equal volumes of Tris-HCl buffer and mechanically homogenized as described above. The lysates were cleared of beads and worm debris (2 times centrifugation at 100 x g for 5 min at 4°C). Equal amounts of worm lysates containing approximately 200  $\mu$ g total protein were then ultracentrifuged at 350,000 x g for 15 min. The supernatant was collected as the Tris-HCl soluble fraction and the resulting pellet was sequentially re-suspended by sonication in 1. Tris-HCl buffer with 1% Triton X-100, 2. Tris-HCl buffer with 1% sarkosyl (Sigma-Aldrich, 61743), and 3. Tris-HCl buffer with SDS sample buffer containing 2% SDS (Carl Roth, CN30.2), each extraction step followed by centrifugation at 350,000 x g for 15 min, resulting in a Triton X-100 soluble fraction, sarkosyl soluble fraction and SDS soluble fraction, respectively. 1/20 of the Tris-HCl soluble fractions, and 1/5 of the Triton X-100, sarkosyl and SDS soluble fractions were subjected to SDS-PAGE and western blotting as detailed above.

### RNAi by feeding and RNAi screen

RNAi experiments were performed by feeding nematodes with *E. coli* HT115(DE3) bacteria expressing target-gene

dsRNA, which were retrieved from the Ahringer RNAi library (Source BioScience, 3318\_Cel\_RNAi\_complete) [108]. RNAi plates were seeded with 200  $\mu$ l of overnight (~14 h) RNAi bacteria cultures, pre-induced with 1 mM IPTG for 3 h. L1 larvae (approx. 40 animals) were transferred onto dried RNAi bacteria seeded plates and grown at 20°C. For the RNAi screen, any effect on the SNCA containing vesicular structures in body wall muscle (BWM) cells relative to the empty vector control was scored in at least 30 animals for each RNAi clone ( $n \geq 3$ ). Moreover, the number of animals that exhibit SNCA::RFP staining in neighboring hypodermal tissue was determined in at least 30 animals for each condition ( $n \geq 3$ ). Experiments were performed blind as to the identity of the RNAi clone, whenever possible. The RNAi experiments with animals expressing SNCA::RFP in dopaminergic neurons were performed as described above with the following modifications: to enhance RNAi efficiency in neurons, we used a strain that is hypersensitive to systemic neuronal RNAi [109].

### LGALS3/galectin-3 puncta assay

Lysosomal membrane permeabilization (LMP) was analyzed by the LGALS3/galectin-3 puncta assay [53]. Animals were age-synchronized and the number of human LGALS3 fused to superfolder GFP (sfGFP::LGALS3) in BWM cells was determined using a Leica DMI8SD AF spinning disc microscope (Leica Microsystems, Germany). At least 20 muscle cells of 20 different animals of each strain were analyzed in each of 4 independent experiments. For hypodermal expression of sfGFP::LGALS3, the number of animals harboring more than 5 or 10 sfGFP::LGALS3 foci in the hypodermis was determined using a Leica M205 FA fluorescence stereomicroscope (Leica Microsystems, Germany). At least 20 animals per strain were analyzed in each of 4 independent experiments.

### Behavioral analysis

#### Thrashing assay

In order to evaluate the physiological consequences of SNCA expression, the function of BWM cells was assessed by a thrashing assay. Age-synchronized animals were transferred from NGM growth plates into M9 buffer. After the animals had become accustomed to the new environment for 1 min, the swimming speed was determined by counting the number of swimming movements (thrashes) within 30 s. One thrash was defined as the entire motion from one side to the other. 10–15 worms were examined for each strain in 3 biological replicates.

#### Basal slowing response assay

The experimental procedure for the basal slowing response assay, which assesses integrity of dopaminergic circuits in *C. elegans*, was adapted from Sawin et al. [110]. Strains were synchronized via egg laying and cultivated on fresh OP50 seeded plates until they reached the desired ages. Seeded assay plates were prepared as follows on the day before analysis; 20  $\mu$ l of OP50 bacteria were added onto 60 mm plates and spread in circular shape using the bottom of a glass



culture tube and incubated overnight at 37°C. This generated plates with a ring-shaped bacterial lawn with a central area of approximately 1 cm in diameter without bacteria. The synchronized progeny at the respective stage of development were first washed 3 times in S-basal buffer to remove residual OP50 and then transferred into the center of such an assay plate in a drop of buffer (5 to 10 animals per plate), which was then gently absorbed using a Kimwipe. In parallel, worms were transferred to an unseeded OP50 plate following the same procedure. Both seeded and unseeded assay plates were then left undisturbed for 5 min, before the number of anterior body bends in a 20 s interval were determined for each worm on the seeded and unseeded assay plates. The relative change in the number of body bends (seeded subtracted from unseeded) was determined in 4 independent repeats of the assay, 2 of which were done blinded. Animals with intact dopaminergic neurons will slow down when encountering the bacterial lawn, whereas animals with impaired dopaminergic neuron function will not slow down. As a positive control, *cat-2*(n4547) mutant animals lacking CAT-2, a homolog for tyrosine hydroxylase, the rate limiting enzyme in the synthesis of dopamine, were used (as described in [111]). The BZ555 strain (Caenorhabditis Genetics Center, BZ555), expressing GFP in all 8 dopaminergic neurons under the control of the *dat-1* promoter, was used in this context as a negative control, exhibiting a WT basal slowing response.

### CEP neuron analysis

Age-synchronized animals were imaged using a Leica DMI8SD AF spinning disc microscope as detailed above to examine the 4 dopaminergic cephalic sensilla (CEP) neurons for morphological changes. An animal was scored positive for 'neuronal abnormalities' if CEP neurons exhibited any of the following strong morphological abnormalities [112]: blebbing (at least 3; beading was not considered strong enough), heavy kinks, breaks or aberrant sprouting of axons (see Figure S7 for representative images). Animals that exhibited a loss of at least one CEP neuron (CEP cell body was invisible in fluorescence microscopy) were scored as 'animals with CEP neurodegeneration'. The strain BZ555, which expresses only GFP in DA neurons, showed none of these age-associated aberrations [112] at this early stage of life when the animals were examined (on day 2 to 6 of life). 10–15 animals were examined at each day in 3 independent experiments.

### Statistical analysis

For all experiments, at least 3 biological replicates were obtained for each strain tested. GraphPad Prism software was used to create graphs and to analyze the data. Data are presented as mean  $\pm$  standard error of the mean (SEM) if not otherwise indicated. To determine whether there are statistically significant differences between strains or treatments, the following statistical tests were performed. The two-way analysis of variance (ANOVA) with Bonferroni posttests or Holm-Sidak's multiple comparisons test were used to compare 2 variables (strains and age) with each another. The one-

way ANOVA together with a Dunnett post-test was used to compare every mean to a control mean.

### Acknowledgments

We thank Dr. Richard I. Morimoto for his support during the early stages of this project and Dr. Olivia Casanueva and Dr. Axel Mogk for helpful discussion and constructive comments on this manuscript. The CLEM work and electron microscopy was done by Dr. Charlotta Funaya at the Electron Microscopy Core Facility (EMCF) of Heidelberg University. We would like to acknowledge the EMCF for their support. We further acknowledge the help of Nicholas Xiao with generating the WT and A53T mutant *myo-3p::SNCA::RFP* strains, and the help of Sonja Sinn with integrating the *dat-1p::SNCA::RFP* transgene. We are grateful to Dr. Claire Richardson and Dr. Kang Shen for supplying the strain TV14687 and to Dr. Harald Hutter for sharing the strain VH95. Dr. Xiaochen Wang generously provided nematodes expressing the transgenes *qxIs66* and *qxIs281*. The strain EG6147 was kindly provided by Dr. Erik Jorgensen. The strain B1J34 and a pPD49.26 expression plasmid coding for sfGFP::LGALS3 were a kind gift of Dr. Bin Liu and Dr. Marja Jäättelä. Some strains were provided by the Caenorhabditis Genetics Center (CGC), which is funded by NIH Office of Research Infrastructure Programs (P40 OD010440).

### Disclosure statement

No potential conflict of interest was reported by the authors.

### Funding

This work was supported by the Deutsche Forschungsgemeinschaft under Grant [KI-1988/3-1] and [NeuroCure Excellence Cluster] to J.K., as well as Grant [SFB1036 TP20] to C.N.K., and a Fulbright Association Scholar Award to C.V.

### ORCID

Carl Alexander Sandhof  <http://orcid.org/0000-0001-8692-6987>

### References

- [1] Ben-Zvi A, Miller EA, Morimoto RI. Collapse of proteostasis represents an early molecular event in Caenorhabditis elegans aging. *Proc Natl Acad Sci U S A*. 2009 Sep 1;106(35):14914–14919. PubMed PMID: 19706382; PubMed Central PMCID: PMC2736453.
- [2] David DC, Ollikainen N, Trinidad JC, et al. Widespread protein aggregation as an inherent part of aging in *C. elegans*. *PLoS Biol*. 2010;8(8):e1000450. PubMed PMID: 20711477; PubMed Central PMCID: PMC2919420.
- [3] Lopez-Otin C, Blasco MA, Partridge L, et al. The hallmarks of aging. *Cell*. 2013 Jun 6;153(6):1194–1217. PubMed PMID: 23746838; PubMed Central PMCID: PMC3836174.
- [4] Ilieva H, Polyimenidou M, Cleveland DW. Non-cell autonomous toxicity in neurodegenerative disorders: ALS and beyond. *J Cell Biol*. 2009 Dec 14;187(6):761–772. PubMed PMID: 19951898; PubMed Central PMCID: PMC2806318.
- [5] Garden GA, La Spada AR. Intercellular (mis)communication in neurodegenerative disease. *Neuron*. 2012 Mar 8;73(5):886–901. S0896-6273(12)00179-1 [pii] 10.1016/j.neuron.2012.02.017. PubMed PMID: 22405200; PubMed Central PMCID: PMC3334539. eng.
- [6] Nussbaum-Krammer CI, Morimoto RI. Caenorhabditis elegans as a model system for studying non-cell-autonomous mechanisms in protein-misfolding diseases. *Dis Model Mech*. 2014 Jan;7

- (1):31–39. PubMed PMID: 24396152; PubMed Central PMCID: PMC3882046.
- [7] Lim S, Kim HJ, Kim DK, et al. Non-cell-autonomous actions of alpha-synuclein: implications in glial synucleinopathies. *Prog Neurobiol.* 2018 Oct;169:158–171. PubMed PMID: 30173732.
- [8] Gu XL, Long CX, Sun L, et al. Astrocytic expression of Parkinson's disease-related A53T alpha-synuclein causes neurodegeneration in mice. *Mol Brain.* 2010 Apr 21;3:12. PubMed PMID: 20409326; PubMed Central PMCID: PMC2873589.
- [9] Recasens A, Dehay B. Alpha-synuclein spreading in Parkinson's disease. *Front Neuroanat.* 2014;8:159. PubMed PMID: 25565982; PubMed Central PMCID: PMC4270285.
- [10] Goedert M, Masuda-Suzukake M, Falcon B. Like prions: the propagation of aggregated tau and alpha-synuclein in neurodegeneration. *Brain.* 2017 Feb;140(2):266–278. PubMed PMID: 27658420.
- [11] Sala AJ, Bott LC, Morimoto RI. Shaping proteostasis at the cellular, tissue, and organismal level. *J Cell Biol.* 2017 May 1;216(5):1231–1241. PubMed PMID: 28400444; PubMed Central PMCID: PMC5412572.
- [12] Bar-Lavan Y, Kosolapov L, Frumkin A, et al. Regulation of cellular protein quality control networks in a multicellular organism. *Febs J.* 2012 Feb;279(4):526–531. PubMed PMID: 22177281.
- [13] Droujinine IA, Perrimon N. Defining the interorgan communication network: systemic coordination of organismal cellular processes under homeostasis and localized stress. *Front Cell Infect Microbiol.* 2013;3:82. PubMed PMID: 24312902; PubMed Central PMCID: PMC3832798.
- [14] Owusu-Ansah E, Perrimon N. Stress signaling between organs in metazoa. *Annu Rev Cell Dev Biol.* 2015;31:497–522. PubMed PMID: 26393775.
- [15] Bohnert KA, Kenyon C. A lysosomal switch triggers proteostasis renewal in the immortal *C. elegans* germ lineage. *Nature.* 2017 Nov 30;551(7682):629–633. PubMed PMID: 29168500; PubMed Central PMCID: PMC5936623.
- [16] Fawcett TW, Sylvester SL, Sarge KD, et al. Effects of neurohormonal stress and aging on the activation of mammalian heat shock factor 1. *J Biol Chem.* 1994 Dec 23;269(51):32272–32278. PubMed PMID: 7798227.
- [17] Prahlad V, Cornelius T, Morimoto RI. Regulation of the cellular heat shock response in *Caenorhabditis elegans* by thermosensory neurons. *Science.* 2008 May 9;320(5877):811–814. PubMed PMID: 18467592; PubMed Central PMCID: PMC3429343.
- [18] Taylor RC, Dillin A. XBP-1 is a cell-nonautonomous regulator of stress resistance and longevity. *Cell.* 2013 Jun 20;153(7):1435–1447. PubMed PMID: 23791175.
- [19] Demontis F, Perrimon N. FOXO/4E-BP signaling in *Drosophila* muscles regulates organism-wide proteostasis during aging. *Cell.* 2010 Nov 24;143(5):813–825. PubMed PMID: 21111239; PubMed Central PMCID: PMC3066043.
- [20] Prahlad V, Morimoto RI. Neuronal circuitry regulates the response of *Caenorhabditis elegans* to misfolded proteins. *Proc Natl Acad Sci U S A.* 2011 Aug 23;108(34):14204–14209. PubMed PMID: 21844355; PubMed Central PMCID: PMC3161566.
- [21] van Oosten-Hawle P, Porter RS, Morimoto RI. Regulation of organismal proteostasis by transcellular chaperone signaling. *Cell.* 2013 Jun 6;153(6):1366–1378. PubMed PMID: 23746847.
- [22] Ulgherait M, Rana A, Rera M, et al. AMPK modulates tissue and organismal aging in a non-cell-autonomous manner. *Cell Rep.* 2014 Sep 25;8(6):1767–1780. PubMed PMID: 25199830; PubMed Central PMCID: PMC4177313.
- [23] Douglas PM, Baird NA, Simic MS, et al. Heterotypic signals from neural HSF-1 separate thermotolerance from longevity. *Cell Rep.* 2015 Aug 18;12(7):1196–1204. PubMed PMID: 26257177.
- [24] Davis CH, Kim KY, Bushong EA, et al. Transcellular degradation of axonal mitochondria. *Proc Natl Acad Sci U S A.* 2014 Jul 1;111(26):9633–9638. PubMed PMID: 24979790; PubMed Central PMCID: PMC4084443.
- [25] Melentijevic I, Toth ML, Arnold ML, et al. *C. elegans* neurons jettison protein aggregates and mitochondria under neurotoxic stress. *Nature.* 2017 Feb 16;542(7641):367–371. PubMed PMID: 28178240; PubMed Central PMCID: PMC5336134.
- [26] Madhivanan K, Greiner ER, Alves-Ferreira M, et al. Cellular clearance of circulating transthyretin decreases cell-nonautonomous proteotoxicity in *Caenorhabditis elegans*. *Proc Natl Acad Sci U S A.* 2018 Aug 14;115(33):E7710–E7719. PubMed PMID: 30061394; PubMed Central PMCID: PMC6099907.
- [27] van Ham TJ, Thijssen KL, Breitling R, et al. *C. elegans* model identifies genetic modifiers of alpha-synuclein inclusion formation during aging. *PLoS Genet.* 2008 Mar;4(3):e1000027. PubMed PMID: 18369446; PubMed Central PMCID: PMC2265412.
- [28] Hamamichi S, Rivas RN, Knight AL, et al. Hypothesis-based RNAi screening identifies neuroprotective genes in a Parkinson's disease model. *Proc Natl Acad Sci U S A.* 2008 Jan 15;105(2):728–733. PubMed PMID: 18182484; PubMed Central PMCID: PMC2206604.
- [29] Kuwahara T, Koyama A, Koyama S, et al. A systematic RNAi screen reveals involvement of endocytic pathway in neuronal dysfunction in alpha-synuclein transgenic *C. elegans*. *Hum Mol Genet.* 2008 Oct 1;17(19):2997–3009. PubMed PMID: 18617532.
- [30] Katayama H, Yamamoto A, Mizushima N, et al. GFP-like proteins stably accumulate in lysosomes. *Cell Struct Funct.* 2008;33(1):1–12. PubMed PMID: 18256512.
- [31] Dehay B, Bove J, Rodriguez-Muela N, et al. Pathogenic lysosomal depletion in Parkinson's disease. *J Neurosci.* 2010 Sep 15;30(37):12535–12544. 30/37/12535 [pii]. PubMed PMID: 20844148.
- [32] Ebrahimi-Fakhari D, Cantuti-Castelvetri I, Fan Z, et al. Distinct roles in vivo for the ubiquitin-proteasome system and the autophagy-lysosomal pathway in the degradation of alpha-synuclein. *J Neurosci.* 2011 Oct 12;31(41):14508–14520. PubMed PMID: 21994367; PubMed Central PMCID: PMC3587176.
- [33] Puska G, Lutz MI, Molnar K, et al. Lysosomal response in relation to alpha-synuclein pathology differs between Parkinson's disease and multiple system atrophy. *Neurobiol Dis.* 2018 Jun;114:140–152. PubMed PMID: 29505813.
- [34] Bourdenx M, Bezard E, Dehay B. Lysosomes and alpha-synuclein form a dangerous duet leading to neuronal cell death. *Front Neuroanat.* 2014;8:83. PubMed PMID: 25177278; PubMed Central PMCID: PMC4132369.
- [35] Campbell RE, Tour O, Palmer AE, et al. A monomeric red fluorescent protein. *Proc Natl Acad Sci U S A.* 2002 Jun 11;99(12):7877–7882. PubMed PMID: 12060735; PubMed Central PMCID: PMC122988.
- [36] Nussbaum-Krammer CI, Park KW, Li L, et al. Spreading of a prion domain from cell-to-cell by vesicular transport in *Caenorhabditis elegans*. *PLoS Genet.* 2013 Mar;9(3):e1003351. PubMed PMID: 23555277; PubMed Central PMCID: PMC3610634.
- [37] Kaminski Schierle GS, Bertoncini CW, Chan FTS, et al. A FRET sensor for non-invasive imaging of amyloid formation in vivo. *Chemphyschem.* 2011 Feb 25;12(3):673–680. PubMed PMID: 21308945; PubMed Central PMCID: PMC35402868.
- [38] Michel CH, Kumar S, Pinotsi D, et al. Extracellular monomeric tau protein is sufficient to initiate the spread of tau protein pathology. *J Biol Chem.* 2014 Jan 10;289(2):956–967. PubMed PMID: 24235150; PubMed Central PMCID: PMC3887218.
- [39] Kuwahara T, Tonegawa R, Ito G, et al. Phosphorylation of alpha-synuclein protein at Ser-129 reduces neuronal dysfunction by lowering its membrane binding property in *Caenorhabditis elegans*. *J Biol Chem.* 2012 Mar 2;287(10):7098–7109. PubMed PMID: 22232559; PubMed Central PMCID: PMC3293593.
- [40] Park C, Suh Y, Cuervo AM. Regulated degradation of Chk1 by chaperone-mediated autophagy in response to DNA damage. *Nat Commun.* 2015 Apr 16;6:6823.

- [41] Kukulski W, Schorb M, Welsch S, et al. Precise, correlated fluorescence microscopy and electron tomography of lowicryl sections using fluorescent fiducial markers. *Methods Cell Biol.* **2012**;111:235–257. PubMed PMID: 22857932.
- [42] Liu B, Du H, Rutkowski R, et al. LAAT-1 is the lysosomal lysine/arginine transporter that maintains amino acid homeostasis. *Science.* **2012** Jul 20;337(6092):351–354. PubMed PMID: 22822152; PubMed Central PMCID: PMC3432903.
- [43] Burkhardt JK, McIlvain JM Jr., Sheetz MP, et al. Lytic granules from cytotoxic T cells exhibit kinesin-dependent motility on microtubules in vitro. *J Cell Sci.* **1993** Jan;104(Pt 1):151–162. PubMed PMID: 8449993.
- [44] Schmoranzler J, Simon SM. Role of microtubules in fusion of post-Golgi vesicles to the plasma membrane. *Mol Biol Cell.* **2003** Apr;14(4):1558–1569. PubMed PMID: 12686609; PubMed Central PMCID: PMC153122.
- [45] Richardson CE, Spilker KA, Cueva JG, et al. PTRN-1, a microtubule minus end-binding CAMSAP homolog, promotes microtubule function in *Caenorhabditis elegans* neurons. *eLife.* **2014** Feb 25;3:e01498. PubMed PMID: 24569477; PubMed Central PMCID: PMC3932522.
- [46] Lee HJ, Patel S, Lee SJ. Intravesicular localization and exocytosis of alpha-synuclein and its aggregates. *J Neurosci.* **2005** Jun 22;25(25):6016–6024. PubMed PMID: 15976091.
- [47] Alvarez-Erviti L, Seow Y, Schapira AH, et al. Lysosomal dysfunction increases exosome-mediated alpha-synuclein release and transmission. *Neurobiol Dis.* **2011** Jun;42(3):360–367. PubMed PMID: 21303699; PubMed Central PMCID: PMC3107939.
- [48] Poehler AM, Xiang W, Spitzer P, et al. Autophagy modulates SNCA/alpha-synuclein release, thereby generating a hostile microenvironment. *Autophagy.* **2014**;10(12):2171–2192. PubMed PMID: 25484190; PubMed Central PMCID: PMC4502760.
- [49] Lopes Da Fonseca T, Villar-Pique A, Outeiro TF. The interplay between alpha-synuclein clearance and spreading. *Biomolecules.* **2015** Apr 14;5(2):435–471. PubMed PMID: 25874605; PubMed Central PMCID: PMCPCMC4496680.
- [50] Kramer JM. Basement membranes. In: *Community TCellR*, editor. *WormBook*; **2005**.
- [51] Conway KA, Lee SJ, Rochet JC, et al. Acceleration of oligomerization, not fibrillization, is a shared property of both alpha-synuclein mutations linked to early-onset Parkinson's disease: implications for pathogenesis and therapy. *Proc Natl Acad Sci U S A.* **2000** Jan 18;97(2):571–576. PubMed PMID: 10639120; PubMed Central PMCID: PMC15371.
- [52] Freeman D, Cedillos R, Choyke S, et al. Alpha-synuclein induces lysosomal rupture and cathepsin dependent reactive oxygen species following endocytosis. *PLoS One.* **2013**;8(4):e62143. PubMed PMID: 23634225; PubMed Central PMCID: PMC3636263.
- [53] Aits S, Krickler J, Liu B, et al. Sensitive detection of lysosomal membrane permeabilization by lysosomal galectin puncta assay. *Autophagy.* **2015**;11(8):1408–1424. PubMed PMID: 26114578; PubMed Central PMCID: PMC4590643.
- [54] Flavin WP, Bousset L, Green ZC, et al. Endocytic vesicle rupture is a conserved mechanism of cellular invasion by amyloid proteins. *Acta Neuropathol.* **2017** May 19. 10.1007/s00401-017-1722-x. PubMed PMID: 28527044.
- [55] Abounit S, Bousset L, Loria F, et al. Tunneling nanotubes spread fibrillar alpha-synuclein by intercellular trafficking of lysosomes. *Embo J.* **2016** Oct 04;35(19):2120–2138. PubMed PMID: 27550960; PubMed Central PMCID: PMC5048354.
- [56] Dixon SJ, Roy PJ. Muscle arm development in *Caenorhabditis elegans*. *Development.* **2005** Jul;132(13):3079–3092. PubMed PMID: 15930100.
- [57] Saegusa K, Sato M, Sato K, et al. *Caenorhabditis elegans* chaperonin CCT/TRiC is required for actin and tubulin biogenesis and microvillus formation in intestinal epithelial cells. *Mol Biol Cell.* **2014** Oct 15;25(20):3095–3104. PubMed PMID: 25143409; PubMed Central PMCID: PMC4196862.
- [58] Pavel M, Imarisio S, Menzies FM, et al. CCT complex restricts neuropathogenic protein aggregation via autophagy. *Nat Commun.* **2016** Dec 08;7:13821. PubMed PMID: 27929117; PubMed Central PMCID: PMC5155164 financial interests.
- [59] Liegeois S, Benedetto A, Garnier JM, et al. The V0-ATPase mediates apical secretion of exosomes containing Hedgehog-related proteins in *Caenorhabditis elegans*. *J Cell Biol.* **2006** Jun 19;173(6):949–961. PubMed PMID: 16785323; PubMed Central PMCID: PMC2063919.
- [60] Marshansky V, Futai M. The V-type H<sup>+</sup>-ATPase in vesicular trafficking: targeting, regulation and function. *Curr Opin Cell Biol.* **2008** Aug;20(4):415–426. PubMed PMID: 18511251.
- [61] Tamai K, Tanaka N, Nakano T, et al. Exosome secretion of dendritic cells is regulated by Hrs, an ESCRT-0 protein. *Biochem Biophys Res Commun.* **2010** Aug 27;399(3):384–390. PubMed PMID: 20673754.
- [62] Oh SH, Kim HN, Park HJ, et al. Mesenchymal stem cells inhibit transmission of alpha-synuclein by modulating clathrin-mediated endocytosis in a parkinsonian model. *Cell Rep.* **2016** Feb 2;14(4):835–849. PubMed PMID: 26776513.
- [63] Wu CW, Deonaraine A, Przybysz A, et al. The Skp1 Homologs SKR-1/2 are required for the *Caenorhabditis elegans* SKN-1 Antioxidant/Detoxification response independently of p38 MAPK. *PLoS Genet.* **2016** Oct;12(10):e1006361. PubMed PMID: 27776126; PubMed Central PMCID: PMC5077136.
- [64] Hiramoto K, Murata T, Shimizu K, et al. Role of phosphodiesterase 2 in growth and invasion of human malignant melanoma cells. *Cell Signal.* **2014** Sep;26(9):1807–1817. PubMed PMID: 24705027; PubMed Central PMCID: PMC4174556.
- [65] Matus DQ, Li XY, Durbin S, et al. In vivo identification of regulators of cell invasion across basement membranes. *Sci Signal.* **2010** May 04;3(120):ra35. PubMed PMID: 20442418; PubMed Central PMCID: PMC3917318.
- [66] Knight AL, Yan X, Hamamichi S, et al. The glycolytic enzyme, GPI, is a functionally conserved modifier of dopaminergic neurodegeneration in Parkinson's models. *Cell Metab.* **2014** Jul 1;20(1):145–157. PubMed PMID: 24882066; PubMed Central PMCID: PMCPCMC4097176.
- [67] Li Y, Chen B, Zou W, et al. The lysosomal membrane protein SCAV-3 maintains lysosome integrity and adult longevity. *J Cell Biol.* **2016** Oct 24;215(2):167–185. PubMed PMID: 27810910; PubMed Central PMCID: PMC5084646.
- [68] Settembre C, Zoncu R, Medina DL, et al. A lysosome-to-nucleus signalling mechanism senses and regulates the lysosome via mTOR and TFEB. *Embo J.* **2012** Mar 07;31(5):1095–1108. PubMed PMID: 22343943; PubMed Central PMCID: PMC3298007.
- [69] Mazzulli JR, Zunke F, Isacson O, et al. alpha-Synuclein-induced lysosomal dysfunction occurs through disruptions in protein trafficking in human midbrain synucleinopathy models. *Proc Natl Acad Sci U S A.* **2016** Feb 16;113(7):1931–1936. PubMed PMID: 26839413; PubMed Central PMCID: PMCPCMC4763774.
- [70] Borland H, Vilhardt F. Prelysosomal compartments in the unconventional secretion of amyloidogenic seeds. *Int J Mol Sci.* **2017** Jan 23;18(1). PubMed PMID: 28124989; PubMed Central PMCID: PMC5297856. DOI: 10.3390/ijms18010227.
- [71] Cooper AA, Gitler AD, Cashikar A, et al. Alpha-synuclein blocks ER-Golgi traffic and Rab1 rescues neuron loss in Parkinson's models. *Science.* **2006** Jul 21;313(5785):324–328. PubMed PMID: 16794039; PubMed Central PMCID: PMC1983366.
- [72] Gitler AD, Chesni A, Geddie ML, et al. Alpha-synuclein is part of a diverse and highly conserved interaction network that includes PARK9 and manganese toxicity. *Nat Genet.* **2009** Mar;41(3):308–315. PubMed PMID: 19182805; PubMed Central PMCID: PMCPCMC2683786.
- [73] Mazzulli JR, Xu YH, Sun Y, et al. Gaucher disease glucocerebrosidase and alpha-synuclein form a bidirectional pathogenic loop in synucleinopathies. *Cell.* **2011** Jul 8;146(1):37–52. PubMed PMID: 21700325; PubMed Central PMCID: PMC3132082.
- [74] Bae EJ, Kim DK, Kim C, et al. LRRK2 kinase regulates alpha-synuclein propagation via RAB35 phosphorylation. *Nat Commun.* **2018** Aug 27;9(1):3465. PubMed PMID: 30150626; PubMed Central PMCID: PMCPCMC6110743.



- [75] Emmanouilidou E, Melachroinou K, Roumeliotis T, et al. Cell-produced alpha-synuclein is secreted in a calcium-dependent manner by exosomes and impacts neuronal survival. *J Neurosci*. 2010 May 19;30(20):6838–6851. PubMed PMID: 20484626.
- [76] Jang A, Lee HJ, Suk JE, et al. Non-classical exocytosis of alpha-synuclein is sensitive to folding states and promoted under stress conditions. *J Neurochem*. 2010 Jun;113(5):1263–1274. PubMed PMID: 20345754.
- [77] Danzer KM, Kranich LR, Ruf WP, et al. Exosomal cell-to-cell transmission of alpha synuclein oligomers. *Mol Neurodegener*. 2012;7:42. PubMed PMID: 22920859; PubMed Central PMCID: PMC3483256.
- [78] Kaletsky R, Yao V, Williams A, et al. Transcriptome analysis of adult *Caenorhabditis elegans* cells reveals tissue-specific gene and isoform expression. *PLoS Genet*. 2018 Aug;14(8):e1007559. PubMed PMID: 30096138; PubMed Central PMCID: PMC6105014.
- [79] Shen Q, He B, Lu N, et al. Phagocytic receptor signaling regulates clathrin and epsin-mediated cytoskeletal remodeling during apoptotic cell engulfment in *C. elegans*. *Development*. 2013 Aug;140(15):3230–3243. PubMed PMID: 23861060; PubMed Central PMCID: PMC3931732.
- [80] Liu G, Rogers J, Murphy CT, et al. EGF signalling activates the ubiquitin proteasome system to modulate *C. elegans* lifespan. *Embo J*. 2011 Jun 14;30(15):2990–3003. PubMed PMID: 21673654; PubMed Central PMCID: PMC3160178.
- [81] Labbadia J, Morimoto RI. Repression of the heat shock response is a programmed event at the onset of reproduction. *Mol Cell*. 2015 Aug 20;59(4):639–650. PubMed PMID: 26212459; PubMed Central PMCID: PMC4546525.
- [82] Baird NA, Douglas PM, Simic MS, et al. HSF-1-mediated cytoskeletal integrity determines thermotolerance and life span. *Science*. 2014 Oct 17;346(6207):360–363. PubMed PMID: 25324391; PubMed Central PMCID: PMC4403873.
- [83] Ewald CY, Landis JN, Porter Abate J, et al. Dauer-independent insulin/IGF-1-signalling implicates collagen remodelling in longevity. *Nature*. 2015 Mar 05;519(7541):97–101. PubMed PMID: 25517099; PubMed Central PMCID: PMC4352135.
- [84] Appelqvist H, Waster P, Kagedal K, et al. The lysosome: from waste bag to potential therapeutic target. *J Mol Cell Biol*. 2013 Aug;5(4):214–226. PubMed PMID: 23918283.
- [85] Naegeli KM, Hastie E, Garde A, et al. Cell invasion in vivo via rapid exocytosis of a transient lysosome-derived membrane domain. *Dev Cell*. 2017 Nov 20;43(4):403–417 e10. PubMed PMID: 29161591; PubMed Central PMCID: PMC5726793.
- [86] Walther DM, Kasturi P, Zheng M, et al. Widespread proteome remodeling and aggregation in aging *C. elegans*. *Cell*. 2015 May 7;161(4):919–932. PubMed PMID: 25957690; PubMed Central PMCID: PMC4643853.
- [87] Ries HM, Nussbaum-Krammer C. Shape matters: the complex relationship between aggregation and toxicity in protein-misfolding diseases. *Essays Biochem*. 2016 Oct 15;60(2):181–190. PubMed PMID: 27744334.
- [88] Shields SB, Piper RC. How ubiquitin functions with ESCRTs. *Traffic*. 2011 Oct;12(10):1306–1317. PubMed PMID: 21722280; PubMed Central PMCID: PMC3171646.
- [89] Frand AR, Russel S, Ruvkun G. Functional genomic analysis of *C. elegans* molting. *PLoS Biol*. 2005 Oct;3(10):e312. PubMed PMID: 16122351; PubMed Central PMCID: PMC1233573.
- [90] van der Goot AT, Zhu W, Vazquez-Manrique RP, et al. Delaying aging and the aging-associated decline in protein homeostasis by inhibition of tryptophan degradation. *Proc Natl Acad Sci U S A*. 2012 Sep 11;109(37):14912–14917. PubMed PMID: 22927396; PubMed Central PMCID: PMC3443121.
- [91] van der Goot AT, Nollen EA. Tryptophan metabolism: entering the field of aging and age-related pathologies. *Trends Mol Med*. 2013 Jun;19(6):336–344. PubMed PMID: 23562344.
- [92] Kim DK, Lim HS, Kawasaki I, et al. Anti-aging treatments slow propagation of synucleinopathy by restoring lysosomal function. *Autophagy*. 2016 Oct 02;12(10):1849–1863. PubMed PMID: 27485532; PubMed Central PMCID: PMC5079673.
- [93] Tyson T, Senchuk M, Cooper JF, et al. Novel animal model defines genetic contributions for neuron-to-neuron transfer of alpha-synuclein. *Sci Rep*. 2017 Aug 08;7(1):7506. PubMed PMID: 28790319; PubMed Central PMCID: PMC5548897.
- [94] Serrano-Puebla A, Boya P. Lysosomal membrane permeabilization in cell death: new evidence and implications for health and disease. *Ann N Y Acad Sci*. 2016 May;1371(1):30–44. PubMed PMID: 26599521.
- [95] Sui YT, Bullock KM, Erickson MA, et al. Alpha synuclein is transported into and out of the brain by the blood-brain barrier. *Peptides*. 2014 Dec;62:197–202. PubMed PMID: 25278492; PubMed Central PMCID: PMC4378645.
- [96] Zlokovic BV. Neurovascular pathways to neurodegeneration in Alzheimer's disease and other disorders. *Nat Rev Neurosci*. 2011 Nov 03;12(12):723–738. PubMed PMID: 22048062; PubMed Central PMCID: PMC4036520.
- [97] Gray MT, Woulfe JM. Striatal blood-brain barrier permeability in Parkinson's disease. *J Cereb Blood Flow Metab*. 2015 May;35(5):747–750. PubMed PMID: 25757748; PubMed Central PMCID: PMC4420870.
- [98] Cooper JF, Dues DJ, Spielbauer KK, et al. Delaying aging is neuroprotective in Parkinson's disease: a genetic analysis in *C. elegans* models. *NPJ Parkinsons Dis*. 2015;1:15022. PubMed PMID: 28725688; PubMed Central PMCID: PMC45516561.
- [99] Abeliovich A, Gitler AD. Defects in trafficking bridge Parkinson's disease pathology and genetics. *Nature*. 2016 Nov 10;539(7628):207–216. PubMed PMID: 27830778.
- [100] Wang C, Telpoukhovskaia MA, Bahr BA, et al. Endo-lysosomal dysfunction: a converging mechanism in neurodegenerative diseases. *Curr Opin Neurobiol*. 2018 Feb;48:52–58. PubMed PMID: 29028540.
- [101] Gao S, Casey AE, Sargeant TJ, et al. Genetic variation within endolysosomal system is associated with late-onset Alzheimer's disease. *Brain*. 2018 Sep 1;141(9):2711–2720. PubMed PMID: 30124770.
- [102] Brenner S. The genetics of *Caenorhabditis elegans*. *Genetics*. 1974 May;77(1):71–94. PubMed PMID: 4366476; PubMed Central PMCID: PMC1213120.
- [103] Nussbaum-Krammer CI, Neto MF, Briemann RM et al. Investigating the spreading and toxicity of prion-like proteins using the metazoan model organism *C. elegans*. *J Vis Exp*. 2015;9552321. PubMed PMID: 25591151. DOI:10.3791/52321
- [104] Bounoutas A, O'Hagan R, Chalfie M. The multipurpose 15-protofilament microtubules in *C. elegans* have specific roles in mechanosensation. *Curr Biol*. 2009 Aug 25;19(16):1362–1367. PubMed PMID: 19615905; PubMed Central PMCID: PMC2757273.
- [105] Luisier F, Blu T, Unser M. Image denoising in mixed Poisson-Gaussian noise. *IEEE Trans Image Process*. 2011 Mar;20(3):696–708. PubMed PMID: 20840902.
- [106] Warren SC, Margineanu A, Alibhai D, et al. Rapid global fitting of large fluorescence lifetime imaging microscopy datasets. *PLoS One*. 2013;8(8):e70687. PubMed PMID: 23940626; PubMed Central PMCID: PMC3734241.
- [107] Paul-Gilloteaux P, Heiligenstein X, Belle M, et al. eC-CLEM: flexible multidimensional registration software for correlative microscopies. *Nat Methods*. 2017 Jan 31;14(2):102–103. PubMed PMID: 28139674.
- [108] Kamath RS, Ahringer J. Genome-wide RNAi screening in *Caenorhabditis elegans*. *Methods*. 2003 Aug;30(4):313–321. PubMed PMID: 12828945.

- [109] Calixto A, Chelur D, Topalidou I, et al. Enhanced neuronal RNAi in *C. elegans* using SID-1. *Nat Methods*. 2010 Jul;7(7):554–559. PubMed PMID: 20512143; PubMed Central PMCID: PMC2894993.
- [110] Sawin ER, Ranganathan R, Horvitz HR. *C. elegans* locomotory rate is modulated by the environment through a dopaminergic pathway and by experience through a serotonergic pathway. *Neuron*. 2000 Jun;26(3):619–631. PubMed PMID: 10896158.
- [111] Peres TV, Arantes LP, Miah MR, et al. Role of *Caenorhabditis elegans* AKT-1/2 and SGK-1 in Manganese toxicity. *Neurotox Res*. 2018 Oct;34(3):584–596. PubMed PMID: 29882004; PubMed Central PMCID: PMC6286235.
- [112] Toth ML, Melentijevic I, Shah L, et al. Neurite sprouting and synapse deterioration in the aging *Caenorhabditis elegans* nervous system. *J Neurosci*. 2012 Jun 27;32(26):8778–8790. PubMed PMID: 22745480; PubMed Central PMCID: PMC3427745.